Potential impact of a U.S. climate policy and air quality regulations on future air quality and climate change

Y. H. Lee[1], D. T. Shindell[2], G. Faluvegi[3], and R. W. Pinder[4]
[1] Laboratory for Atmospheric Research, Civil and Environmental Engineering, Washington State University, Pullman, WA, USA
[2] Earth and Ocean Sciences, Nicholas School of the Environment, Duke University, Durham, NC, USA
[3] NASA Goddard Institute for Space Studies and Columbia Earth Institute, New York, NY, USA
[4] NextClimate, Carborro, NC, USA

Abstract

We have investigated how future air quality and climate change are influenced by the U.S. air quality regulations that existed or were proposed in 2013 and a hypothetical climate mitigation policy that aims to reduce 2050 CO_2 emissions to be 50% below 2005 emissions. Using the NASA GISS ModelE2 general circulation model, we look at the impacts in year 2030 and 2055. The U.S. energy-sector emissions are from the GLIMPSE project (GEOS-Chem LIDORT Integrated with MARKAL for the Purpose of Scenario Exploration), and other U.S. emissions datasets and the rest of the world emissions datasets are based on the RCP4.5 scenario. The U.S. air quality regulations are projected to have a strong beneficial impact on U.S. air quality and public health in year 2030 and 2055 but result in positive radiative forcing. Under this scenario, no more emission constraints are added after 2020, and the impacts on air quality and climate change are similar between year 2030 and 2055. Surface PM2.5 is reduced by ~2 μg m^{-3} on average over the U.S., and surface ozone by ~8 ppbv. The improved air quality prevents about 91,400 premature deaths in the US, mainly due to the PM2.5 reduction (~74,200 lives saved). The air quality regulations reduce the light-reflecting aerosols (i.e., sulfate and organic matter) more than the light-absorbing species (i.e., black carbon and ozone), leading to a strong positive radiative forcing (RF) over the US by both aerosols direct and indirect forcing: total RF is ~0.04 W m^{-2} over the globe; ~0.8 W m^{-2} over the US. Under the hypothetical climate policy, future CO_2 emissions cut is achieved in part by relying less on coal, and thus SO_2 emissions are noticeably reduced. This provides air quality co-benefits, but it could lead to potential climate dis-benefits over the US. In 2055, the U.S. mean total RF is +0.22 W m^{-2} due to

positive aerosol direct and indirect forcing, while the global mean total RF is -0.06 W m^{-2} due to the dominant negative CO_2 RF (instantaneous RF). To achieve a regional-scale climate benefit via a climate policy, it is critical 1) to have multi-national efforts to reduce GHGs emissions and 2) to simultaneously target emission reduction of light-absorbing species (e.g., BC and O_3) on top of long-lived species. The latter is very desirable as the resulting climate benefit occurs faster and provides co-benefits to air quality and public health.

1. Introduction

The U.S. Environmental Protection Agency (EPA)'s air quality regulations have historically been focused on air quality assessment in terms of public health and environmental damages. With the Endangerment Finding under the Clean Air Act in December 2009 (U.S. Environmental Protection Agency, 2009), the EPA sought to understand and provide integrated policy approaches to both mitigate climate change and manage air quality (e.g., U.S. Environmental Protection Agency, 2012). This requires estimating potential climate and air quality impacts of various greenhouse gases (GHG) and short-lived climate pollutants (SLCP) including some "traditional" pollutants regulated under the Clean Air Act.

With growing interest in identifying potential energy policy that maximize benefits to air quality and reduce climate change impacts, a rapid decision tool for energy and environmental policy has been developed in the U.S. Environmental Protection Agency: GLIMPSE (GEOS-Chem LIDORT Integrated with MARKAL for the Purpose of Scenario Exploration). Under the GLIMPSE project (http://www.epa.gov/AMD/Research/Climate/GLIMPSE.html; Akhtar et al., 2013), the MARKet ALlocation (MARKAL) optimization model (Fishbone and Abilock, 1981; Loughlin et al., 2011) is used to estimate emissions based on energy policy actions, and the Adjoint GEOS-Chem global chemical transport model and the LIDORT radiative transfer model (Henze et al., 2012) is used to compute the impact of emissions, chemical fate, and transport on direct radiative forcing. The GLIMPSE decision-making tool examines combined constraints of greenhouse gas emissions,

short-lived species direct radiative forcing, and relative cost to examine the trade-offs between different policy options. Akhtar et al. (2013) present the four emission scenarios based on energy policy and air quality regulations and the impact of these emissions on direct radiative forcing and public health: see the description of emission scenarios in Section 2 in this paper.

A major limitation on the climate impact estimates in Akhtar et al. (2013) is that they only use direct radiative forcing of sulfate, black carbon and organic carbon aerosols: no direct forcing by gas pollutants and no aerosol indirect effects. Moreover, their direct radiative forcing estimates cannot account for non-linear behavior in the impact of emissions on direct radiative forcing (an inherent limitation of an adjoint model). In order to get a more complete assessment of climate impact, we investigate the impact of the GLIMPSE emission scenarios using the NASA Goddard Institute for Space Studies (GISS) ModelE2 general circulation model, i.e., a fully coupled atmospheric chemistry-climate model. We utilize two independent aerosol models coupled to the same GISS ModelE2 climate model to obtain a more robust estimate of aerosol impacts on air quality and climate. Using an entirely different air quality model than Akhtar et al. (2013), our study provides an independent analysis for the air quality component of the impact of the same GLIMPSE emission scenarios.

The paper is organized as follows. Section 2 provides the detailed descriptions of the four emission scenarios developed from GLIMPSE. The NASA GISS ModelE2 description, including a bulk aerosol model and a sectional aerosol microphysics model, is provided in Section 3. In section 4, we present the model results and discussions including the changes of gases and aerosols budgets and their radiative forcing under the four scenarios. Conclusions are in Section 5.

2. Scenarios Descriptions

To identify the climate and health impacts of US emission reductions, four energy sector scenarios were developed using the Market Allocation optimization (MARKAL) model and are described in detail in Akhtar et al. (2013). Each scenario is

specified as a set of emission constraints. MARKAL finds the least-cost set of energy technologies that meet US energy demands while not exceeding the specified emission constraints. Output from MARKAL includes both energy technologies and associated emissions for air pollutants and greenhouse gases. For example, if a scenario is specified only as a reduction in CO_2 emissions, and the least-cost way to achieve those emission reductions included less coal combustion for electricity generation, the results from MARKAL would include the reductions in emissions of SO_2, NO_X, and related air pollutants from coal combustion. Emissions from sources other than the energy sector are from the RCP (Representative Concentration Pathway) 4.5 scenario (Thomson et al., 2011). Here we describe each scenario briefly (see Fig. 1 for the emission trajectories of SO_2, Black Carbon (BC), Organic Carbon (OC), CH_4, CO, NO_X, Alkenes and Paraffin from 2005 to 2055).

2.1 Baseline (bs)

This bs emission scenario (blue solid line in Fig. 1) is based on the U.S. air quality regulations affecting the electricity sector and the transportation sector. For example, it includes Clean Air Interstate Rule (CAIR), state-level renewable portfolio standards (RPSs), the new Corporate Average Fuel Economy (CAFE) standard, Tier II light duty emission standards, heavy-duty engine emission standards, and diesel sulfur limits (see Akhtar et al. 2013; the details of each regulation can be found in https://www3.epa.gov/air/oarregul.html). The scenario does not assume any future air quality regulations beyond those that existed or were proposed in 2013. After 2020, there are no more emission constraints added. No CO_2 specific regulation, such as the Clean Power Plan, is included in this scenario though CO_2 emissions are influenced indirectly by some of the regulations included here. These regulations do not lead to a significant change in energy sources or the amount of electricity. Natural gas is added when needing additional electricity, and coal, nuclear, and renewable electricity production remain at approximately current level. Notably, the CO_2 emission rate in 2055 is almost same as 2005 in this scenario, partly because growing energy usage due to higher demands is offset by better fuel efficiency.

2.2 No air quality regulations (noaq)

This noaq emission scenario (red solid line in Fig. 1) removes existing and proposed air quality regulations, which means no emission reduction strategies. Under this scenario, most pollutant emissions either stay similar to their 2005 level or increase slightly by 2055. Similar to the bs scenario, there is no effort to reduce CO_2 emissions.

2.3 50% CO_2 cap in the bs scenario (c50)

This c50 emission scenario (blue dashed line in Fig. 1) is the same as the bs scenario, but additionally includes a hypothetical climate change mitigation target, which applies a linear reduction in CO_2 emissions from the 2005 level at 2005 to 50% of 2005 levels at 2050 (called "50% CO_2 cap"). With the 50% CO_2 cap, there are major fuel source changes in the electricity sector: switching from coal-power plants to natural gas-fired plants, applying carbon sequestration technology for all fossil fuel production, and increasing wind/solar power based on regional source availability. The 50% CO_2 cap applied in the US contributes about 10% reduction in the global CO_2 emissions of the RCP4.5 scenario in 2050.

Starting in 2020, the 50% CO_2 cap results in less SO_2 and OC emissions but more BC emissions compared to the air quality regulation (i.e., the bs scenario). Note that larger BC emissions are due to increased biomass fuel usage in the residential, commercial, and industrial sectors as a bridge fuel. CO emissions are also slightly reduced but only after 2040.

2.4 50% CO_2 cap in the noaq scenario (c50nq)

This c50nq emission scenario (red dashed line in Fig. 1) is the same as the noaq scenario, but includes the 50% CO_2 cap. This scenario also leads to significant changes in energy sources and electricity production by 2055. For some pollutants, the impact of the 50% CO_2 cap can be quite different under the noaq scenario than the bs scenario. For instance, SO_2 emissions are significantly reduced under this scenario mainly because of retiring coal-power plants, which have high SO_2 emissions. Without the air quality regulations, the SO_2 emission reductions result solely from the 50% CO_2 cap, and thus occurs more slowly over time than in the c50 scenario (e.g., the SO_2 emission reductions reach to the bs scenario level in 2040).

Except for CH_4, most gas pollutant emissions deviate from the noaq scenario after around 2040.

Note that the US emission scenarios are not same in year 2005, even though they may appear so in Fig. 1. For instance, the bs emissions are not identical to the c50 emissions in year 2005.

3. Model descriptions

We used two independent aerosol models that coupled to the same host climate model, NASA GISS ModelE2 (Schmidt et al., 2014): ModelE2-OMA (One Moment Aerosol model with no aerosol microphysics) and ModelE2-TOMAS (TwO-Moment Aerosol Sectional) microphysics model. The host climate model has 2° latitude by 2.5° longitude resolution, with 40 vertical hybrid sigma layers from the surface to 0.1 hPa (80 km). Tracers, heat, and humidity are advected using the highly nondiffusive Quadratic Upstream Scheme (Prather, 1986). The radiation scheme accounts for size-dependent scattering properties of clouds and aerosols based on Mie scattering (Hansen et al., 1983) and non-spherical light scattering of cirrus and dust particles based on T-matrix theory (Mishchenko et al., 1996). In the model, clouds are distinguished into convective and large-scale stratiform clouds. The clouds parameterizations are similar to Del Genio (Del Genio et al., 1996; Del Genio and Yao, 1993) but have been improved in several respects (see details in Schmidt et al., 2006, 2014). The physics time-step is 30 minutes, and the radiation calculations are performed every 2.5 hours.

ModelE2-OMA uses a default aerosol module, which has no aerosol microphysics such as coagulation, condensation and nucleation and thus does not calculate aerosol size distributions. ModelE2-OMA simulates sulfate, carbonaceous aerosols, secondary organic aerosols, nitrate, sea-salt (two size classes with a fine mode, 0.1 to 1 μm in dry radii, and a coarse mode, 1 to 4 μm in dry radii) and mineral dust (five size classes for clay, 0.1 and 1 μm in dry radii, and four size classes for silts, 1 to 16 μm in dry radii) aerosols as well as sulfur dioxide, dimethyl sulfide (DMS), methanesulfonic acid (MSA), isoprene, monoterpenes, and sesquiterpenes aerosol

precursor gases (see details in Schmidt et al., 2014). Heterogeneous chemistry on the surfaces of mineral dust particles is included to form nitrate and sulfate (Bauer and Koch, 2005). Dry deposition is based on a resistance-in-series scheme, and wet deposition is determined by scavenging within and below clouds, scavenging by precipitations, and evaporation of clouds and precipitating water (Koch et al., 2006). ModelE2-OMA computes a dissolved species budget for large-scale clouds, so some sulfate formed in clouds undergoes wet scavenging without being released in air (Koch et al., 2006). Aerosol-cloud interaction is based on an empirical parameterization that computes cloud droplet number concentrations as a function of aerosol mass (Menon et al., 2002, 2008).

ModelE2-TOMAS uses a sectional aerosol microphysics approach that tracks two moments of the aerosol size distribution in each size section or "bin": total aerosol number (i.e., 0^{th} moment) and mass (i.e., 1^{st} mass moment). A detailed description of the TOMAS microphysics algorithm is in Adams and Seinfeld (2002) and Lee and Adams (2012). We used TOMAS with 15 bins covering 3 nm to 10 μm. Aerosol mass in each size bin is decomposed into nine aerosol species: sulphate mass, sea-salt mass, mass of pure (hydrophobic) elemental carbon (EC), mass of mixed (aged) EC, mass of hydrophobic organic matter (OM), mass of hydrophilic OM, mass of mineral dust, mass of ammonium and mass of water. In addition, the model tracks four bulk gas-phase species: sulphur dioxide (SO_2), dimethylsulfide (DMS), sulphuric acid (H_2SO_4), and a lumped gas-phase tracer that represents oxidized organic vapours forming secondary organic aerosol (SOA). TOMAS accounts for water uptake by hydrophilic OM, sulphate and sea salt. We use binary nucleation (Vehkamaki et al., 2002) with sulfuric acid concentrations reduced by five times and no additional boundary-layer nucleation because it tends to overpredict aerosol number concentrations in ModelE2-TOMAS (Lee et al., 2015). This might be related to overpredicted sulfur dioxide lifted into the upper and free troposphere over the Pacific Ocean in ModelE2, possibly due to overly-strong convective transport, which can be oxidized to form sulfuric acid and then contribute to nucleation (Lee et al., 2015). Dry and wet deposition in ModelE2-TOMAS are similar to those in ModelE2-OMA, but, when needed, using size-dependent processes such as gravitational

settling, size-dependent resistance in the quasi-laminar sublayer (Adams and Seinfeld, 2002; Seinfeld and Pandis, 1998), a modified Köhler theory for in-cloud scavenging (Pierce et al., 2007) and a modified first-order removal scheme for below-cloud scavenging (Adams and Seinfeld, 2002). For the aerosol-cloud interactions, we compute a critical supersaturation and cloud droplet number concentrations (CDNC) using a physical-based activation parameterization from Nenes and Seinfeld (2003) with feeding a model updraft velocity that is computed based on a large-scale vertical velocity and sub-grid velocity. In ModelE2-TOMAS, size-resolved AOD is computed using a volume-averaged refractive index, based on Mie theory.

Both ModelE2-OMA and ModelE2-TOMAS use the same tropospheric and stratospheric gas chemistry model, which includes 156 chemical reactions among 51 gas species (Shindell et al., 2013a). In ModelE2, gas chemistry and aerosols are interactive, which means aerosol chemistry is computed with online oxidant fields (e.g., H_2O_2, OH, and NO_3 for sulfur aerosol; see Bell et al., 2005b). Photolysis rates are computed using the Fast-J2 scheme (), and aerosol optical depth in ModelE2-OMA affects photolysis rates (not for ModelE2-TOMAS). Ozone in the ModelE2 was previously evaluated in Shindell et al (2013a), which found that around 900 hPa ozone tended to be overpredicted in the model by around 5-8 ppbv. Though ozone in this version of the model was improved at higher altitudes, values near the surface were similar to the prior ModelE, which displayed little mean bias relative to a network of 40 surface ozone measurements although the correlation was only R=0.7 (Shindell et al., 2006). The atmospheric residence time of methane in modelE2 is in excellent agreement with the value inferred from observations, indicating that OH levels are also well simulated. Additional analysis of seasonal maximum 8-hourly surface ozone showed that the model captures the summertime observed levels in the western US very well, but substantially overestimates values in eastern North America (Schnell et al., 2015)

The detailed description and evaluation of ModelE2-TOMAS and the difference between OMA and TOMAS is available in Lee et al. (2014). In brief, the ModelE2-TOMAS and ModelE2-OMA models capture the observed sulfur species and other

aerosol species as well as aerosol optical depth mostly within a factor of two. However, anthropogenic aerosols in both models differ from each other by a few percent to a factor of 2 regionally due to differences in aerosol processes such as deposition, cloud processing, and emission parameterizations.

The climate impact of each scenario is based on radiative forcing estimated using ModelE2, except for CO_2 RF. Since ModelE2 does not simulate a carbon cycle and cannot estimate the CO_2 RF as result of CO_2 emission changes, we use the same approach as Collins et al. (2013), which utilizes the CO_2 impulse response function representing the multiple timescales involved in the carbon cycle as in the 2007 IPCC Assessment (Forster et al., 2007). The impulse response function characterizes the complex behavior of the climate response to CO_2 emission changes as a first-order approximation. Due to the linear system assumption in the function, it has a limitation on representing non-linear and path dependent processes (e.g., Joos et al., 2013). However, CO_2 emission changes in our scenarios are much smaller than 1 Gt C per year whereas an impulse response function is likely in a linear regime when the CO_2 impulse size is below 100 Gt C (Joos et al., 2013; Olivié and Peters, 2013). Nevertheless, in order to estimate the variation in CO_2 RF associated with the choice of an impulse response function, we have estimated CO_2 RF using additional impulse response functions derived from multi-model intercomparison projects such as C^4MIP and CMIP5, which are obtained from Olivié and Peters (2013). We found that our CO_2 RF differs only by 3-4% when using the impulse response functions fitted to the multi-model mean of CMIP5 and by 10-17% when using impulse response functions fitted to the multi-model mean of C^4MIP.

Both ModelE2-OMA and ModelE2-TOMAS have participated various inter-comparisons studies for global-scale atmospheric chemistry models such as the Atmospheric Chemistry and Climate Model Intercomparison Project (ACCMIP) and AeroCom (e.g., Lamarque et al., 2013; Lee et al., 2013; Mann et al., 2014; Naik et al., 2013; Shindell et al., 2013b).

3.1. Simulation setup

All simulations were performed as timeslices with three years spin-up, targeting year 2005, 2030, and 2055. Aerosols and short-lived gases emissions were from the given time period. Three types of simulations were performed to isolate the impact due to emissions changes alone from other factors such future warm climate conditions and rapid adjustments as a result of the emission changes. A brief description of simulations is provided in Table 1, and the detailed description is below.

In order to assess the impact of each emission scenario on air quality and climate, we set our climate model to have identical meteorology among all emission scenarios by 1) disabling the influence of aerosols and gases on radiation and clouds in the model (i.e., turning off aerosols-climate and gases-climate interactions) and 2) prescribing observed monthly mean sea surface temperatures (SST) and sea ice (SICE) coverage averaged from 2001 to 2010 in all FIXMET runs. We denote these simulations as FIXMET. Since the model meteorology is identical, emissions are the only contributing factor to the difference among the runs. This type of run is used here because the impact of U.S. emissions on radiative forcing is likely too small to distinguish from model internal noise that can be large via clouds. We performed three-year simulations for FIXMET because the model meteorology is identical among the simulations and their year-to-year variation is small enough. Our FIXMET simulations with ModelE2-OMA were run with a newer ModelE2 version, which included some updates relative to ModelE2-TOMAS because nitrate aerosols in ModelE2-OMA were unrealistically high in the same version of ModelE2 as ModelE2-TOMAS (Lee et al., 2015; Shindell et al., 2013b).

Since future warm climate alone can have a significant impact on gas pollutants (e.g., O_3, CO, NO_X, and CH_4), we ran FIXMET 2030 and 2055 simulations but with prescribed monthly mean SST and SICE from 2026-2034 and 2051-2059 means from ModelE2 RCP4.5 simulations, respectively. We denote these runs as FUTURE.

Finally, we ran simulations with allowing aerosols and gases to interact with radiation and clouds (referred to as INTERACT runs) to find out the impact of

emission controls including the atmospheric response to emissions. The same SST and SICE fields used for FIXMET were also used in these simulations. With this fixed SST method, we can estimate the radiative response following "rapid" adjustments in the atmosphere due to a forcing agent. It is important to note that this method has been used to estimate aerosol effective forcing (e.g., Shindell et al., 2013b), but only allowing aerosol emissions changes from the reference period. In this study, both aerosol and gas emissions are changed from the reference period (i.e., 2005) and the resulting cloud radiative forcing is also influenced by gas forcing. Thus it cannot be used to estimate aerosol effective forcing. We performed the runs for 20 years to remove the model internal noise.

The ModelE2 version used in this study does not compute CH_4 RF with simulated concentrations, if the CH_4-radiation interactions are turned off, which is the case in the FIXMET and FUTURE simulations. Thus, we use CH_4 RF from the INTERACT simulations and other RFs from the FIXMET simulations in Section 4.3. This inconsistency would little influence to overall RFs, since the CH_4 RF signal is small compared to other RFs.

3.2. Air quality related mortality calculations

We calculated the health impacts of air pollutants as premature deaths due to increased lung cancer (LC), cardiovascular disease (CVD), and respiratory disease and infections (RESP) for PM2.5 exposure, based on concentration-response functions (CRF) derived from epidemiological studies. For O_3 exposure, CVD and RESP are used to compute annual mortality. The change in premature deaths is calculated using Eq. (1):

$$\Delta M = M_b \cdot P \cdot AF \qquad \text{Eq. (1)}$$

where M is the number of premature deaths due to PM2.5 or O_3, M_b is the cause-specific baseline mortality rate, P is the relevant population, and AF is the attributable fraction of premature deaths due to PM2.5 or O_3 exposure, which is defined as:

$$AF = (RR-1)/RR \qquad \text{Eq. (2)}$$

where RR is relative risk of death from a cause-specific disease (i.e., LC, CVD, or RESP) as a result of exposure to PM2.5 or ozone increase. RRs are the main parameter estimated from epidemiological studies, but are subject to a large uncertainty.

To characterize the uncertainties in CRF, we used three different CRF equations (called $CRF_{low,pm}$, $CRF_{base,pm}$, and $CRF_{high,pm}$) to compute PM2.5-related mortality and two different equations ($CRF_{low,o3}$ and $CRF_{base,o3}$) for O_3-related mortality. For PM2.5-related mortality, we used annual mean PM2.5 concentrations that exclude sea-salt and dust aerosols. Since 1) sea-salt and dust aerosols are mostly naturally emitted and highly varied due to wind-dependence of their emissions and 2) the toxicity of sea-salt and dust particles is weaker than anthropogenic aerosols (Anenberg et al., 2012), the health impact of a policy-driven measure is obtained without them. For O_3-related mortality, we used simulated hourly surface ozone concentrations for $CRF_{low,O3}$ and $CRF_{high,O3}$. We summarize the key equations and parameters for each CRF below and in Table 2.

Our CRF_{base} ($CRF_{base,\ pm}$ and $CRF_{base,o3}$) method is based on the case 1 in Anenberg et al. (2012), which computes RR using $\exp(\beta\Delta C)$; where β is the estimated slope of the log-linear relationship between PM2.5 or O_3 and premature deaths, and ΔC is the change in PM2.5 or O_3. The $CRF_{base,pm}$ is based on long-term RR derived from an American Cancer Society (ACS) cohort study (Pope et al., 2002): Every 10-$\mu g\ m^{-3}$ increase in PM2.5 is associated with 14% and 9% increases in LC and CVD/RESP mortality, respectively. However, Anenberg et al. (2012) increase the RRs from Pope et al. (2002) by 1.8 to scale up to the mean of the expert elicitation (Roman et al., 2008). Epidemiological studies indicate that the CRF slope derived from U.S. data is log-linear over the concentration range from low to ~40 ug m-3 [Krewski et al., 2009; Laden et al., 2006]. This suggests that the $CRF_{base,pm}$ (i.e., log-linear CRF) might be most appropriate for the US. For O_3, $CRF_{base,o3}$ uses long-term RR from the ACS cohort (Jerrett et al., 2009): every 10-ppb increase in the seasonal (6-month) average of 1-hr daily maximum O_3 is associated with a 4% increase in respiratory disease mortality.

The $CRF_{high,pm}$ is based on the case 2 in Anenberg et al., (2012), which uses a log CRF from Pope et al. (2002). In this method, pre-scaling β is 0.2322 and 0.1552 for LC and CVD/RESP, respectively, following Cohen et al. (2004). These are scaled, as in the CRF_{base} case, by a factor of 1.8. The RR in $CRF_{high,pm}$ is computed using changes in log of PM2.5 (ΔlnC). Compared to the other CRFs used here, this tends to predict larger changes in premature deaths (thus, we name it $CRF_{high,pm}$).

Our CRF_{low} ($CRF_{low,pm}$ and $CRF_{low,o3}$) is based on Marlier et al. (2013). For $CRF_{low,pm}$, a power-law relationship is assumed between premature death and high PM2.5, including cigarette and ambient pollution, following Pope et al. (2011). The RRs for PM2.5 in this method are computed quite differently: as a function of the PM2.5 concentration rather than the concentration change; see the equations in Table 2. Note that $CRF_{low,pm}$ does not include PM2.5-related premature deaths caused by RESP. This CRF tends to predict the smallest change in premature deaths among the three CRFs used here. For $CRF_{low,o3}$, a log-linear relationship is assumed between O_3 and premature deaths with 1.11 for β, based on Bell et al., (2005a): a 10 ppb increase in daily-averaged O_3 concentrations is associated with 11% increase in cardiovascular disease mortality.

We use baseline mortality rates (M_b in Eq.1) for all persons age 15 and older from the World Health Organization (available via http://www.who.int/healthinfo/global_burden_disease/estimates_country_2004_2008). For all health calculations, to obtain the relevant population (P in Eq 1), we use the year 2005 population data from the Center for International Earth Science Information Network (2005) and scale on a per country basis to obtain population for people age 30 or older, based on United Nations Population Division (2011) estimates. This inconsistency in age limit (ages 15+ in Mb vs. 30+ in P) is inevitable due to the coarseness of age categories in the mortality data, but any bias from this inconsistency is expected to be small compared to the differences across CRFs. We would like to mention that our health impacts can be computed with future populations, scaled by country from the 2015 gridded population using a medium fertility scenario (United Nations Population Division, 2011). In this study, we

confine the mortality change to air quality causes, rather than population changes, so a year 2005 population data is used for all cases. Economic impacts can also be computed, but are not shown in this paper.

As the horizontal resolution in our model is relatively coarse, we redistribute the BC and OM components of simulated PM2.5 output in a model 2 x 2.5 grid cell onto a 0.5 x 0.5 grid, using a subgrid parameterization of urban/rural differences developed by the European Commission's Joint Research Center. This approach has been used in previous studies (Anenberg et al., 2012; Shindell et al., 2011, 2012). The downscaled surface PM2.5 was used to estimate the PM-related mortality rate.

4. Impact of the air quality regulations and CO_2 reduction policy

We estimate the changes in air quality and radiative forcing due to the US air quality regulations and a hypothetical CO_2 reduction target, using the FIXMET runs (see Table 3 for our method). The changes from the FIXMET runs are entirely due to the emissions and do not include any impact of the rapid atmospheric adjustments due to the emissions or future warming climate conditions. We present the results from 2030 and 2055 simulations relative to the 2005 simulations, as indicated in Table 3, i.e., 2030-2005 and 2055-2005. We use acronyms for simulations used to assess the impact of the air quality regulations and CO_2 reduction policy: the simulations used to obtain the impact of the air quality regulation in 2030 and 2055 are denoted as AQ30 and AQ55, respectively; for the impact of CO_2 reduction policy in the presence of the air quality regulations as $CO_2$30 and $CO_2$55; for the impact of CO_2 reduction policy in the absence of air quality regulations as CO_2NQ30 and CO_2NQ55; for the impact of both air quality regulation and CO_2 reduction policy as BOTH30 and BOTH55 (see Table 3 for the exact pair of simulations used for each case). We performed the FIXMET runs with ModelE2-OMA and ModelE2-TOMAS. Since the emission perturbation is over the US continent, we mainly examine a change over the US. It is important to mention that all 50 states are used for air quality and public health estimates but only 48 states excluding Alaska and Hawaii

for radiative forcing. The magnitudes of air quality and mortality rate changes are larger when excluding Hawaii and Alaska, as the two states have relatively clean air.

4.1. Air pollution

Air pollution is mainly examined using the simulated PM2.5, CO, O_3, and NO_x in the model surface air. Along with total PM2.5, we also present a chemical composition of PM2.5 such as sulfate (SU), black carbon (BC), organic matter (OM), and nitrate (NO_3). Using the model surface air pollutant concentrations, PM-related and ozone-related mortality rates are computed.

We examine the impact of the air quality regulations and CO_2 reduction policy on air pollution using US averages (Figure 2) and a spatial distribution over the globe (Figure 3). Since no more emission constraints are added after 2020, impacts on air quality in 2030 and 2055 are quite similar (see Figs 1 and 2). Due to this, Fig. 3 presents only the 2030-2005 cases. To emphasize the future air quality changes over the U.S. in 2030 and 2055, the 2005 baseline air quality level (i.e., bs05 run) is used as a reference (see Table 4). In other words, the impact of policies is divided by the bs05 air quality level (e.g., AQ30/bs05): the bs05 level is presented in S-Table 1 in the supplementary materials.

Figures 2 and 3 show a large improvement in U.S. air quality in 2030 and 2055 due to the air quality regulations (i.e, AQ30, AQ55, BOTH30, and BOTH55). For PM2.5 in Fig. 2, the air quality regulations lead to about 1.5-2.5 $\mu g\ m^{-3}$ reduction in 2030 and 2055, which is about 20-25% of the bs05 PM2.5 concentrations. All aerosol types (SU, BC, OM, and NO_3) are reduced by roughly 30-60% of the bs05 level. Due to the air quality regulations, surface PM2.5 is reduced over the continental US (especially eastern US) and neighboring areas significantly and somewhat slightly over Eurasia (0.01-0.1 $\mu g\ m^{-3}$) due to less long-range transport of US-origin PM and PM precursor gases. Gas pollutants such as O_3, VOC, NO_X, and CO are also effectively reduced: on U.S. average, ~8 ppb for surface O_3 (~15% of the bs05 level); ~2 ppb for NO_X (60-70% of the bs05 level); ~20-25 ppb for CO (~10% of the bs05 level). The spatial distributions reveal that NO_X changes are mostly localized over the North America but O_3 and CO are reduced more than 1 ppb

throughout the Northern Hemisphere (NH) due to the longer lifetime of these pollutants.

For the CO_2 reduction policy (i.e., $CO_2$30. $CO_2$55, CO_2NQ30, and CO_2NQ55), impacts on air pollution are more complex than those of the air quality regulations. Firstly, except for SO_4, most pollutants show a distinct spatial pattern driven by emissions, i.e., increasing concentrations over the southeastern US and decreasing concentrations over the northwestern US. The changes in energy sources under the CO_2 policy differ by each region (depending on regionally specific conditions). For instance, the increases over the south central US states can be explained by the increases in energy production. In 2030, these US states reduces their coal usage and the adoptions of renewable energy such as solar and wind power happens after 2030. Thus, SO_4 is the only air pollutant strongly reduced under the CO_2 reduction policy in 2030 over the south central US. Secondly, since the CO_2 emissions are gradually reduced until 2050, larger impacts are predicted in 2055 than 2030. Also, the changes in an air pollutant are not always same between 2030 and 2055, in term of magnitude and sign of the changes. Ozone is initially increased slightly in 2030 but then decreased in 2055, following the emissions trend of the precursor gases (NO_X, CO and VOC) (Fig.1). However, the changes in O_3 by the CO_2 policy are quite small. For surface PM2.5, it is reduced both in 2030 and 2055, mainly due to SO_2 emission reductions via the fuel switch from coal to renewable energy resources. Interestingly, despite the expected anti-correlation between nitrate and sulfate formation via thermodynamics, nitrate is reduced along with sulfate possibly because of the stronger influences of NO_X emissions reductions (in Fig. 3, the spatial distribution of nitrate closely follows that of NO_X). Lastly, impacts of measures targeting CO_2 on air quality are larger in the absence of the air quality regulations (i.e., CO_2NQ), because using less coal reduces SO_2 emissions effectively without the air quality regulations. For instance, when the air quality regulations are applied (i.e., $CO_2$30 and $CO_2$55), the U.S. averaged PM2.5 concentration is reduced by 0.13-0.34 $\mu g\ m^{-3}$ (about 1-5% of the bs05 level) mainly driven by sulfate reduction. Without the air quality regulation (i.e., CO_2NQ30 and CO_2NQ55), PM2.5 is reduced

by 0.36-0.81 μg m^{-3} (about 5-10% of the bs05 level). To be clear, the absolute pollution level is higher in the CO_2NQ cases than the CO_2 cases. In the case of O_3 in 2055, the CO_2NQ55 case shows a reduction (-1.1 ppbv) while the $CO_2$55 case shows a slight increase (+0.03 ppbv). The same pattern is also observed in ModelE2-TOMAS.

The results presented above are based on ModelE2-OMA. Using ModelE2-TOMAS aerosol microphysics model, we observe similar changes in air pollutions by the air quality regulations and CO_2 reduction policy (see Fig. 4). However, there are some differences in the magnitudes of their PM2.5 changes, largely due to missing nitrate aerosols in ModelE2-TOMAS (only ModelE2-OMA simulates nitrate particles). Besides the nitrates, ModelE2-TOMAS tends to simulate more sulfate reduction and less OM reduction. These effects cancel each other and overall PM2.5 difference between the models is almost equivalent to the amount of nitrate shown in Fig. 2. The changes in gas pollutants are very similar between the models, as the same gas chemistry module is used for both models.

4.2. Health Impacts

Figure 5 shows the number of prevented PM2.5-related premature deaths in the US due to LC, CVD, and RESP by the impact of the air quality regulations and CO_2 reduction policy. Based on $CRF_{base,PM}$, the PM2.5 reduction with the air quality regulations prevents about 74,200 and 78,500 deaths over the U.S in 2030 and 2055, respectively. For the CO_2 reduction policy, about 5,500 and 19,600 PM2.5-related deaths are avoided in 2030 and 2055, respectively. Since the CO_2 policy improves air quality more significantly in later years, the prevented deaths in 2055 are much larger than that in 2030. As discussed in Section 4.1, the relative impact of the CO_2 reduction policy on air quality is larger without the air quality regulations (i.e., CO_2NQ30 and CO_2NQ55). Thus, the prevented deaths are about 2-3 times larger under the CO_2NQ cases: ~17,100 vs. ~5,500 in 2030 and ~36,100 vs. ~19,600 in 2055. We find that there is about an order of magnitude a difference in total mortality rate between $CRF_{low,PM}$ and $CRF_{high,PM}$, indicating large uncertainties in CRF methods. However, all CRF cases show that CVD is the major contributor to overall

PM2.5-related mortality, and the contributions by LC and RESP are quite similar to each other.

The O_3-related premature deaths are presented in Figure 6. Based on the $CRF_{base,o3}$ method that includes only RESP, the air quality regulations prevent about 17,200-18,400 deaths over the U.S. in 2030 and 2055, while the CO_2 reduction policy leads to ~1,600 fewer deaths in 2030 and ~400 deaths in 2055. However, the CO_2NQ case prevents ~2,700 deaths in 2055, following the surface O_3 trends discussed in Section 4.1. Compared to $CRF_{base,O3}$, $CRF_{low,O3}$ includes mortality due to CVD and overall mortality computed with this method is about a factor of two less. For the premature deaths owing to RESP, the two CRF methods are different by 1.5-2 orders of magnitude.

The US mortality rates contribute global mortality rate approximately 80-90% of PM-related mortality and 30-40% for O_3-related mortality (see S-Table 4 in the supplementary materials for the global mortality rate). Compared to PM, the benefits of controlling US ozone precursor emissions are being spread out to the NH region, as ozone is a secondary air pollutant with a longer lifetime than aerosol constituents. For AQ30, $CO_2$30, and $CO_2$55, its global distributions are presented in Figs 7a, 7d, and 7g, respectively. Note that the spatial distribution in AQ55 is almost identical to AQ30 (not shown). Eastern US shows the strongest changes in mortality. There are noticeable impacts over Canada, Mexico, European and Asian countries but no impacts on the Southern Hemisphere. Unlike $CO_2$55, $CO_2$30 shows increasing mortality in the Southeastern US due to the increase in O_3, BC, OM, and NO_3 aerosols (see Fig. 3).

Figure 8 shows the difference between ModelE2-TOMAS and ModelE2-OMA in overall PM-related mortality estimated from three CRF methods, i.e., (ModelE2-TOMAS – ModelE2-OMA). The sign of mortality changes generally agrees well between the two aerosol models, but they are different in term of the magnitudes. For instance, the AQ and BOTH cases with the air quality regulations result in significantly less number of prevented deaths in all CRF approaches using ModelE2-TOMAS: ~25% less prevented deaths for $CRF_{low,PM}$; ~40% for $CRF_{base,PM}$; ~15% for $CRF_{high,PM}$. This is due to missing nitrate aerosol in ModelE2-TOMAS, which leads

more than half of PM2.5 reduction in ModelE2-OMA. We note that the cases of $CO_2$30 and CO_2NQ55 in Fig. 8 show inconsistent changes among the CRF approaches, which is a result of having non-linearity in each CRF.

For the AQ30, $CO_2$30, and $CO_2$55 cases, the spatial distributions of the model differences are shown in Fig. 7. ModelE2-TOMAS tends to simulate lower number of prevented PM-related deaths over the US but larger deaths over some part of Eurasia including India. For ModelE2-TOMAS, despite the increase in BC and OM in the $CO_2$30 case, the premature deaths are reduced everywhere in the US because SO_4 decrease is stronger than the combined BC and OM increase (thus, a different spatial pattern than ModelE2-OMA). It demonstrates how uncertainties in aerosol modeling can play an important role, emphasizing the importance of utilizing more than one aerosol models for estimating health benefits from pollutant emission controls.

4.3. Climate impacts

We estimate the climate impact using aerosol direct forcing (ADF), aerosol first indirect forcing (AIF), BC-albedo forcing, ozone RF (radiative forcing), methane RF, and CO_2 RF in this study. Note that the ozone RFs are referenced at the tropopause, where they provide a better indicator of global temperature response, while the others are at the top of atmosphere. Figure 9 presents individual RF averaged over the globe as well as over the U.S. (48 states only) in 2030 and 2055 relative to 2005. Note that BC-albedo forcing is added to ADF in Fig. 9, and AIF and ozone RF are from the FIXMET runs, methane RF from the INTERACT runs, CO_2 RF from the simple carbon cycle model, and total RF is summed over all aerosols, ozone, methane and CO_2. The RF spatial distributions in 2030 relative to 2005 are presented in Fig. 10 for the impact of CO_2 reduction policy and in Fig. 11 for the impact of the air quality regulations. The RF spatial distributions in 2055 are very similar to those in 2033 (not shown).

In the case of the impact of CO_2 policy in the presence of the air quality regulation (the CO_2 cases), both ADF and AIF are positive throughout the globe

(0.009 W m^{-2} as the global mean) due to reduction of light-reflecting species such as SO_4, OM, and NO_3. Sum of ozone and methane RFs is negligible in both global and US means because their RFs are small and cancelled each other. There is overall negative RF globally (-0.015 W m^{-2} in 2030 and -0.056 W m^{-2} in 2055) but positive over the US regions (0.14 W m^{-2} in 2030 and 0.22 W m^{-2} in 2055) because of positive aerosol RF. The localized aerosol RFs is due to its short lifetime, while the well-distributed negative CO_2 RF over the globe is due to its long lifetime. The strong positive RF from aerosols are mostly localized over the U.S. especially over the eastern US (in Figure 10 for the 2030 case). Previous studies show a large influence of regional RF on the regional climate response (i.e., surface air temperature) over the US (Leibensperger et al., 2012) or the NH mid-latitude regions (Shindell and Faluvegi, 2009). Our regional RF over the US is only 0.22 W m-2 in 2055 and therefore the resulting climate response would be small. Nevertheless it is likely to contribute to warming rather than cooling at least in the near term and thus the CO_2 reduction policy used in our study could potentially lead to mild regional climate dis-benefits over the US, especially during the summer (Shindell et al., 2016). For the CO_2 reduction policy in the absence of the air quality regulation (the CO_2NQ cases), total RF is slightly more positive than the CO_2 cases due to larger reduction in SO_2 emissions.

Since the air quality regulations remove light-reflecting species more effectively than light-absorbing species without affecting CO_2 RF, total RF is positive both globally (0.035 W m^{-2} in 2030 and 0.036 W m^{-2} in 2055) and U.S. regionally (0.83 W m^{-2} in 2030 and 0.82 W m^{-2} in 2055). Note again that the impact of the air quality regulations is quite similar between 2030 and 2055, so the 2055 cases are not shown. In Fig. 11, the light-reflecting aerosols such as SO_4 and OM show a positive RF, and the light-absorbing species such as BC and O_3 show a negative RF. In 2030 relative to 2005, overall ADF is positive (global mean, 0.023 W m^{-2}; US mean, 0.55 W m^{-2}) mainly due to dominant positive RF by sulfate, and AIF is also positive (global mean, 0.029 W m^{-2}; US mean, 0.38 W m^{-2}) due to reduced cloud droplet number concentrations (CDNC). We find the US air quality regulations have a moderate impact on radiative forcing over the Atlantic Ocean and the Pacific Ocean nearby

California, roughly 0.1~0.5 W m^{-2} in 2030, and a mild impact throughout the NH, roughly 0.01~0.05 W m^{-2}. We also find that the magnitude of AIF is comparable to that of ADF, which means it is critical to include the AIF to assess the climate impact of an emission policy.

Compared to ModelE2-OMA, overall RF in ModelE2-TOMAS tends to be less positive in most cases, which can be mainly explained by the difference in sulfate, nitrate, and aerosol indirect effects. The global mean and US mean RF values are presented in S-Tables 5 and 6 for ModelE2-OMA and S-Tables 7 and 8 for ModelE2-TOMAS, respectively. Given that the difference in nitrate is simply due to missing it in ModelE2-TOMAS, we focus on the model difference in sulfate and AIF. Regardless of emission scenarios, ModelE2-OMA simulates more positive sulfate ADF than ModelE2-TOMAS for both global and US means. For AIF, ModelE2-OMA tend to predict more positive AIF both global and US means in all scenarios except for the US mean of the CO_2 and CO_2NQ cases. It is worth note that the differences of surface PM between the two aerosol models shown in Fig. 4 cannot explain the RF differences. For example, the US mean surface nitrate is reduced under these scenarios but the US mean nitrate ADF is negative. Since aerosol RFs (and aerosol optical depth) depend on a vertical distribution of aerosols and assumed aerosol optical properties, the surface PM alone are not sufficient to explain RFs.

5. Impact of future climate conditions and rapid adjustments

We discover that the impact of policies on radiative forcing over the US is affected only a little by using the future climate conditions (i.e., FUTURE runs). As shown in Fig. 13, ADF averaged over the US (including BC-albedo RF, which is much weaker than ADF) is generally less positive than that in the FIXMET runs (shown in Fig. 9), and the changes are a few percent. US mean AIF is more strongly influenced by the future climate conditions, becoming more positive by 20-40% from the FIXMET runs. Ozone RF is changed less than 10% except for the CO_2 policy cases.

Looking at the individual scenario (e.g., bs30, bs55, c5030, c5055; not by the policies), the impact of future climate condition is quite similar among the scenarios,

which lead to increase ADF (including BC-albedo RF) by 0.12-0.17 W m^{-2} and O_3 RF by 0.07-0.1 W m^{-2} and to decrease AIF by 1.9-2.1 W m^{-2} over the US. The positive O_3 RF can be explained by increased O_3 in the middle and upper troposphere (where its radiative forcing per unit change is largest) that closely follows NO_X changes, which might be explained by the fact that the lightning NO_x sources are increased by 10-14% in 2030 and 2055, compared to in 2005. We find that surface ozone is decreased with a warmer future climate over most of the globe (including the US) except for a few areas such as Eastern Europe, India and Southeast Asia where surface ozone pollution is particularly high in the model (not shown). This suggests that future warm climates tend to lead to less ozone in most areas due to increased loss of reactive oxygen with water vapor, and more ozone in highly polluted areas related to increased thermal decomposition of PANs, both of which are consistent with the finding by Doherty et al. (2013). There is some disagreement with the GISS GCM model results presented in Doherty et al. (2013) in term of the detailed spatial patterns of the changes in ozone pollution due to the warmer temperatures, which is not surprising given the difference in emission scenarios (year 2001 TF-HTAP emissions used for Doherty et al. (2013) whereas year 2030/2055 RCP4.5 emissions used in this study).

Using the INTERACT runs, we find that no large changes in ADF and ozone RF are found by allowing model climate/meteorology to be influenced by aerosols and gases (shown in Fig. 14). Nevertheless, we observe some systematic changes such as a) the impact of the atmospheric rapid adjustments on O_3 RF is relatively large under the CO_2 reduction policy (i.e., $CO_2$30. $CO_2$55, CO_2NQ30, and CO_2NQ55), and b) the relative changes are larger in O_3 RF than ADF. The latter is also shown in the FUTURE simulations, and this might be due to the fact that O_3 is a greenhouse gas that interacts with the outgoing longwave radiations which depends on temperature whereas the aerosols interact with only solar radiation via aerosol direct effects in our forcing calculation. For example, in the $CO_2$30 cases, ADF increases by 26%, whereas O_3 RF decreases by 3 times. In the case of AQ30, ADF decreases by 8% while O_3 RF increased by 54%. Note that AIF is not included here because the cloud

radiative forcing in the INTERACT runs is also influenced by gas tracers such as ozone and methane.

6. Conclusions

We have investigated the impact of future U.S. emission scenarios, based on air quality regulations and a hypothetical CO_2 reduction target, on air quality, public health and climate change. The four GLIMPSE emission scenarios developed from the U.S. EPA are used here, which are hypothetical scenarios with and without the air quality regulations and/or a climate policy that reduces the 2005 U.S. CO_2 emissions by 50% by 2050 (see Akhtar et al., 2013). We have performed various simulations with these scenarios, using the NASA GISS ModelE2 climate model with default aerosol model (ModelE2-OMA; no aerosol microphysics model in ModelE2; Schmidt et al., 2014). To find out the uncertainties in aerosol modeling, we have used the sectional-based aerosol microphysics model (ModelE2-TOMAS; Lee et al., 2015) that also coupled to the NASA GISS ModelE2. Since the host climate model is identical, the differences in their results originate solely from the differences in aerosol modeling.

We have found that the U.S. air quality regulations are projected to have a strong beneficial impact on U.S. air quality and public health in the future but result in a positive local radiative forcing. For U.S. air quality, we find significant reduction across the pollutant species: on average, ~2 μg m^{-3} reduction for surface PM2.5; ~8 ppbv reduction for surface O_3. We observe a slight reduction of surface PM2.5 in Eurasia (0.01-0.1 μg m^{-3}) and more than 1 ppbv reduction in surface O_3 throughout the NH. Based on the CRF_{base} (most appropriate CRF for U.S), the improved air quality prevents about 91,400 premature deaths in the US, which is combined from ~74,200 and ~17,200 deaths as a result of the PM2.5 and O_3 reductions, respectively. However, the estimate is significantly affected by the choice of the CRFs (e.g., a factor of two less with the CRF_{low} case and a factor of 4-5 higher using the CRF_{high} case), indicating that the mortality estimate is very sensitive to the uncertainties in the concentration-response functions. The air quality regulations

have strong climate dis-benefits over the U.S., resulting in an overall RF of ~0.8 W m^{-2}, which is strongly positive due to reflective aerosols.

We have discovered that the CO_2 reduction policy has some benefit to air quality via reducing SO_2 emissions. Under this policy, the US relies less on coal, which reduces SO_2 emissions significantly. Surface PM2.5 is reduced by 0.4 μg m^{-3} on average over the continental U.S. in year 2055, which is about 20% of the impact of air quality regulations (0.4 vs. 2 μg m^{-3}). According to our estimates with CRF_{base}, it prevents ~19,200 premature deaths (~19,600 deaths for PM2.5 decrease and ~-400 deaths for O_3 increase); ozone is slightly increased in 2055 but it is almost negligible. This indicates that a potentially substantial benefit associated with air quality improvement takes place under the CO_2 reduction policy. Our findings agree well with other studies showing air quality co-benefits of a climate policy (e.g., Groosman et al., 2011; Nemet et al., 2010; Thompson et al., 2014). These studies estimate a substantial cost benefit when the health benefits resulted from a CO2 policy is monetized. For instance, Thompson et al. (2014) find that the monetized health co-benefits can be greater than the climate policy implementation costs.

In our study, the CO_2 reduction policy results in a net cooling on a global-scale due to the loss of cooling aerosols, but the policy leads to a net positive forcing over the US on a regional scale. Under the CO_2 reduction policy, future US energy resources come less from coal (thus, reducing SO_2 emissions), which is the main reason for reducing the health impacts from air pollution, but, at the same time, could lead to climate dis-benefits over the US potentially. In the year 2055 (when U.S. CO_2 emissions reach half of their 2005 emissions), the U.S. mean total RF is +0.22 W m^{-2} due to aerosol RF, while the global mean total RF is -0.06 W m^{-2} due to the dominant negative CO_2 RF (instantaneous RF). Using the equilibrium CO_2 RF (i.e., year 2150), the CO_2 RF increases from -0.07 W m_{-2} to -0.17 W m_{-2}, but still it is not large enough to cancel the positive forcing from aerosols in U.S regions.

Utilizing two independent aerosol models in the same host GCM, we have found that overall conclusions agree well between the two aerosol models, but missing species such as nitrate can influence the air quality and climate impact moderately.

Our climate estimates reinforce that aerosol RF is a dominant forcing agent for regional climate change, and AIF is as important as ADF. A climate impact only based on aerosol direct forcing can be misleading, and we strongly suggest including AIF for more complete assessment of the climate impact of emission scenarios. Since our study utilized a single host GCM, and we recognize that there are large model-to-model differences among GCMs (e.g., Shindell et al., 2013b), we encourage other modeling groups to perform similar work using other host GCMs, to obtain more robust results.

Due to their long lifetime of CO_2 (or other long-lived GHGs), the climate benefit from a local CO_2 emission reduction is spread spatially (over large areas) and temporally (occurs slowly). This is why it is difficult to achieve regional-scale short-term climate benefits with the CO_2 reduction policy alone. It is important to mention that air quality and health co-benefits from the climate policies could be potentially substantial, and these benefits are immediate and hence within a timeframe relevant for policymakers.

There are a few options that could help to achieve regional-scale climate benefits under a climate policy. First, as discussed by Akhtar et al. (2013), setting the 50% CO_2 cap in an earlier year than 2030 can help to reduce regional warming by bringing the cooling effects of reductions in CO_2 emissions sooner (so that the climate system would have less time to respond to the near-term warming from aerosol reductions). Second, our hypothetical CO_2 reduction policy does not target CH_4 emissions reductions, but if there is CH_4 mitigation, it would lead to a considerable climate benefit both globally and regionally. Rogelj et al. (2015) shows a potentially large climate benefit by very stringent CH_4 mitigations, although these might be extremely ambitious. Lastly, all nations taking action to reduce long-lived GHGs emissions is the clearest way to achieve regional-scale climate benefits. Along with CO_2 reductions, a more comprehensive climate policy with additional reduction targets for light-absorbing aerosols and gases (SLCPs; e.g., BC, CH_4 and O_3) would help to achieve additional regional climate benefits while increasing the co-benefits to air quality and public health.

Acknowledgements

The authors thank Dan Loughlin for assistance with interpreting emission scenarios developed using MARKAL. Also, the authors acknowledge Farhan Akhtar in Department of State for his contribution to GLIMPSE project; preparing the GLIMPSE emissions files for ModelE2 and providing useful comments for this manuscript.

References

Adams, P. J. and Seinfeld, J. H.: Predicting global aerosol size distributions in general circulation models, J. Geophys. Res.-Atmospheres, 107, 4370, doi:doi:10.1029/2001JD001010, 2002.

Akhtar, F. H., Pinder, R. W., Loughlin, D. H. and Henze, D. K.: GLIMPSE: A Rapid Decision Framework for Energy and Environmental Policy, Environ. Sci. Technol., 47(21), 12011–12019, doi:10.1021/es402283j, 2013.

Anenberg, S. C., Schwartz, J., Shindell, D., Amann, M., Faluvegi, G., Klimont, Z., Janssens-Maenhout, G., Pozzoli, L., Van Dingenen, R., Vignati, E., Emberson, L., Muller, N. Z., West, J. J., Williams, M., Demkine, V., Hicks, W. K., Kuylenstierna, J., Raes, F. and Ramanathan, V.: Global Air Quality and Health Co-benefits of Mitigating Near-Term Climate Change through Methane and Black Carbon Emission Controls, Environ. Health Perspect., 120(6), 831–839, doi:10.1289/ehp.1104301, 2012.

Bauer, S. E. and Koch, D.: Impact of heterogeneous sulfate formation at mineral dust surfaces on aerosol loads and radiative forcing in the Goddard Institute for Space Studies general circulation model, J. Geophys. Res.-Atmospheres, 110, D17, doi:doi: 10.1029/2005jd005870, 2005.

Bell, M. L., Dominici, F. and Samet, J. M.: A Meta-Analysis of Time-Series Studies of Ozone and Mortality With Comparison to the National Morbidity, Mortality, and Air Pollution Study, Epidemiol. Camb. Mass, 16(4), 436–445, 2005a.

Bell, N., Koch, D. and Shindell, D. T.: Impacts of chemistry-aerosol coupling on tropospheric ozone and sulfate simulations in a general circulation model, J. Geophys. Res. Atmospheres, 110(D14), D14305, doi:10.1029/2004JD005538, 2005b.

Center for International Earth Science Information Network - CIESIN - Columbia University and Centro Internacional de Agricultura Tropical - CIAT: Gridded

Population of the World, Version 3 (GPWv3): Population Density Grid, Future Estimates, [online] Available from: http://dx.doi.org/10.7927/H4ST7MRB, 2005.

Cohen, A., Anderson, H. R., Ostro, B., Pandey, K. D., Krzyzanowski, M., Künzli, N., Gutschmidt, K., Pope III, C. A., Romieu, I., Samset, J. M. and Smith, K. R.: Urban air pollution, in Comparative Quantification of Health Risks: Global and Regional Burden of Disease due to Selected Major Risk Factors (Ezzati M, Lopez AD, Rodgers A, Murray CJL, eds), pp. 1353–1434, World Health Organization. [online] Available from: http://www.who.int/publications/cra/chapters/volume2/1353-1434.pdf (Accessed 9 September 2015), 2004.

Collins, W. J., Fry, M. M., Yu, H., Fuglestvedt, J. S., Shindell, D. T. and West, J. J.: Global and regional temperature-change potentials for near-term climate forcers, Atmos Chem Phys, 13(5), 2471–2485, doi:10.5194/acp-13-2471-2013, 2013.

Del Genio, A. D. and Yao, M.-S.: Efficient Cumulus Parameterization for Long-Term Climate Studies: The GISS Scheme, in The Representation of Cumulus Convection in Numerical Models, edited by K. A. Emanuel and D. J. Raymond, pp. 181–184, American Meteorological Society. [online] Available from: http://link.springer.com/chapter/10.1007/978-1-935704-13-3_18 (Accessed 7 August 2015), 1993.

Del Genio, A. D., Yao, M.-S., Kovari, W. and Lo, K. K.-W.: A Prognostic Cloud Water Parameterization for Global Climate Models, J. Clim., 9(2), 270–304, doi:10.1175/1520-0442(1996)009<0270:APCWPF>2.0.CO;2, 1996.

Doherty, R. M., Wild, O., Shindell, D. T., Zeng, G., MacKenzie, I. A., Collins, W. J., Fiore, A. M., Stevenson, D. S., Dentener, F. J., Schultz, M. G., Hess, P., Derwent, R. G. and Keating, T. J.: Impacts of climate change on surface ozone and intercontinental ozone pollution: A multi-model study, J. Geophys. Res. Atmospheres, 118(9), 3744–3763, doi:10.1002/jgrd.50266, 2013.

Fishbone, L. G. and Abilock, H.: Markal, a linear-programming model for energy systems analysis: Technical description of the bnl version, Int. J. Energy Res., 5(4), 353–375, doi:10.1002/er.4440050406, 1981.

Forster, P., Ramaswamy, V., Artaxo, P., Berntsen, T., Betts, R., Fahey, D. W., Haywood, J., Lean, J., Lowe, D. C., Myhre, G., Nganga, J., Prinn, R., Raga, G., Schulz, M. and Van Dorland, R.: Changes in Atmospheric Constituents and in Radiative Forcing. Chapter 2, [online] Available from: http://inis.iaea.org/Search/search.aspx?orig_q=RN:39002468 (Accessed 7 August 2015), 2007.

Groosman, B., Muller, N. Z. and O'Neill-Toy, E.: The Ancillary Benefits from Climate Policy in the United States, Environ. Resour. Econ., 50(4), 585–603, doi:10.1007/s10640-011-9483-9, 2011.

Hansen, J., Russell, G., Rind, D., Stone, P., Lacis, A., Lebedeff, S., Ruedy, R. and Travis, L.: Efficient 3-Dimensional Global-Models for Climate Studies - Model-I and Model-Ii, Mon. Weather Rev., 111(4), 609–662, 1983.

Henze, D. K., Shindell, D. T., Akhtar, F., Spurr, R. J. D., Pinder, R. W., Loughlin, D., Kopacz, M., Singh, K. and Shim, C.: Spatially Refined Aerosol Direct Radiative Forcing Efficiencies, Environ. Sci. Technol., 46(17), 9511–9518, doi:10.1021/es301993s, 2012.

Jerrett, M., Burnett, R. T., Pope, C. A., Ito, K., Thurston, G., Krewski, D., Shi, Y., Calle, E. and Thun, M.: Long-Term Ozone Exposure and Mortality, N. Engl. J. Med., 360(11), 1085–1095, doi:10.1056/NEJMoa0803894, 2009.

Joos, F., Roth, R., Fuglestvedt, J. S., Peters, G. P., Enting, I. G., von Bloh, W., Brovkin, V., Burke, E. J., Eby, M., Edwards, N. R., Friedrich, T., Frölicher, T. L., Halloran, P. R., Holden, P. B., Jones, C., Kleinen, T., Mackenzie, F. T., Matsumoto, K., Meinshausen, M., Plattner, G.-K., Reisinger, A., Segschneider, J., Shaffer, G., Steinacher, M., Strassmann, K., Tanaka, K., Timmermann, A. and Weaver, A. J.: Carbon dioxide and climate impulse response functions for the computation of greenhouse gas metrics: a multi-model analysis, Atmos Chem Phys, 13(5), 2793–2825, doi:10.5194/acp-13-2793-2013, 2013.

Koch, D., Schmidt, G. A. and Field, C. V.: Sulfur, sea salt, and radionuclide aerosols in GISS ModelE, J. Geophys. Res.-Atmospheres, 111(D6), doi:doi:10.1029/2004jd005550, 2006.

Krewski, D., Jerrett, M., Burnett, R. T., Ma, R., Hughes, E., Shi, Y., Turner, M. C., Pope 3rd, C. A., Thurston, G., Calle, E. E., Thun, M. J., Beckerman, B., DeLuca, P., Finkelstein, N., Ito, K., Moore, D. K., Newbold, K. B., Ramsay, T., Ross, Z., Shin, H. and Tempalski, B.: Extended follow-up and spatial analysis of the American Cancer Society study linking particulate air pollution and mortality, Res. Rep. Health Eff. Inst., (140), 5–36, 2009.

Laden, F., Schwartz, J., Speizer, F. E. and Dockery, D. W.: Reduction in fine particulate air pollution and mortality: Extended follow-up of the Harvard Six Cities study, Am. J. Respir. Crit. Care Med., 173(6), 667–672, doi:10.1164/rccm.200503-443OC, 2006.

Lamarque, J.-F., Dentener, F., McConnell, J., Ro, C.-U., Shaw, M., Vet, R., Bergmann, D., Cameron-Smith, P., Dalsoren, S., Doherty, R., Faluvegi, G., Ghan, S. J., Josse, B., Lee, Y. H., MacKenzie, I. A., Plummer, D., Shindell, D. T., Skeie, R. B., Stevenson, D. S., Strode, S., Zeng, G., Curran, M., Dahl-Jensen, D., Das, S., Fritzsche, D. and Nolan, M.: Multi-model mean nitrogen and sulfur deposition from the Atmospheric Chemistry and Climate Model Intercomparison Project (ACCMIP): evaluation of historical and projected future changes, Atmos Chem Phys, 13(16), 7997–8018, doi:10.5194/acp-13-7997-2013, 2013.

Lee, Y. H. and Adams, P. J.: A Fast and Efficient Version of the TwO-Moment Aerosol Sectional (TOMAS) Global Aerosol Microphysics Model, Aerosol Sci. Technol., 46(6), 678–689, doi:10.1080/02786826.2011.643259, 2012.

Lee, Y. H., Lamarque, J. F., Flanner, M. G., Jiao, C., Shindell, D. T., Berntsen, T., Bisiaux, M. M., Cao, J., Collins, W. J., Curran, M., Edwards, R., Faluvegi, G., Ghan, S., Horowitz, L. W., McConnell, J. R., Ming, J., Myhre, G., Nagashima, T., Naik, V., Rumbold, S. T., Skeie, R. B., Sudo, K., Takemura, T., Thevenon, F., Xu, B. and Yoon, J. H.: Evaluation of preindustrial to present-day black carbon and its albedo forcing from Atmospheric Chemistry and Climate Model Intercomparison Project (ACCMIP), Atmospheric Chem. Phys., 13(5), 2607–2634, doi:10.5194/acp-13-2607-2013, 2013.

Lee, Y. H., Adams, P. J. and Shindell, D. T.: Evaluation of the global aerosol microphysical ModelE2-TOMAS model against satellite and ground-based observations, Geosci Model Dev, 8(3), 631–667, doi:10.5194/gmd-8-631-2015, 2015.

Leibensperger, E. M., Mickley, L. J., Jacob, D. J., Chen, W. T., Seinfeld, J. H., Nenes, A., Adams, P. J., Streets, D. G., Kumar, N. and Rind, D.: Climatic effects of 1950-2050 changes in US anthropogenic aerosols - Part 2: Climate response, Atmospheric Chem. Phys., 12(7), 3349–3362, doi:10.5194/acp-12-3349-2012, 2012.

Loughlin, D. H., Benjey, W. G. and Nolte, C. G.: ESP v1.0: methodology for exploring emission impacts of future scenarios in the United States, Geosci Model Dev, 4(2), 287–297, doi:10.5194/gmd-4-287-2011, 2011.

Mann, G. W., Carslaw, K. S., Reddington, C. L., Pringle, K. J., Schulz, M., Asmi, A., Spracklen, D. V., Ridley, D. A., Woodhouse, M. T., Lee, L. A., Zhang, K., Ghan, S. J., Easter, R. C., Liu, X., Stier, P., Lee, Y. H., Adams, P. J., Tost, H., Lelieveld, J., Bauer, S. E., Tsigaridis, K., van Noije, T. P. C., Strunk, A., Vignati, E., Bellouin, N., Dalvi, M., Johnson, C. E., Bergman, T., Kokkola, H., von Salzen, K., Yu, F., Luo, G., Petzold, A., Heintzenberg, J., Clarke, A., Ogren, J. A., Gras, J., Baltensperger, U., Kaminski, U., Jennings, S. G., O'Dowd, C. D., Harrison, R. M., Beddows, D. C. S., Kulmala, M., Viisanen, Y., Ulevicius, V., Mihalopoulos, N., Zdimal, V., Fiebig, M., Hansson, H.-C., Swietlicki, E. and Henzing, J. S.: Intercomparison and evaluation of global aerosol microphysical properties among AeroCom models of a range of complexity, Atmos Chem Phys, 14(9), 4679–4713, doi:10.5194/acp-14-4679-2014, 2014.

Marlier, M. E., DeFries, R. S., Voulgarakis, A., Kinney, P. L., Randerson, J. T., Shindell, D. T., Chen, Y. and Faluvegi, G.: El Nino and health risks from landscape fire emissions in southeast Asia, Nat. Clim. Change, 3(2), 131–136, doi:10.1038/nclimate1658, 2013.

Menon, S., Del Genio, A. D., Koch, D. and Tselioudis, G.: GCM Simulations of the aerosol indirect effect: Sensitivity to cloud parameterization and aerosol burden, J. Atmospheric Sci., 59(3), 692–713, doi:10.1175/1520-0469(2002)059<0692:gsotai>2.0.co;2, 2002.

Menon, S., Del Genio, A. D., Kaufman, Y., Bennartz, R., Koch, D., Loeb, N. and Orlikowski, D.: Analyzing signatures of aerosol-cloud interactions from satellite retrievals and the GISS GCM to constrain the aerosol indirect effect, J. Geophys. Res.-Atmospheres, 113(D14), doi:D14s22 10.1029/2007jd009442, 2008.

Mishchenko, M. I., Travis, L. D. and Mackowski, D. W.: T-matrix computations of light scattering by nonspherical particles: A review, J. Quant. Spectrosc. Radiat. Transf., 55(5), 535–575, doi:10.1016/0022-4073(96)00002-7, 1996.

Naik, V., Voulgarakis, A., Fiore, A. M., Horowitz, L. W., Lamarque, J.-F., Lin, M., Prather, M. J., Young, P. J., Bergmann, D., Cameron-Smith, P. J., Cionni, I., Collins, W. J., Dalsøren, S. B., Doherty, R., Eyring, V., Faluvegi, G., Folberth, G. A., Josse, B., Lee, Y. H., MacKenzie, I. A., Nagashima, T., van Noije, T. P. C., Plummer, D. A., Righi, M., Rumbold, S. T., Skeie, R., Shindell, D. T., Stevenson, D. S., Strode, S., Sudo, K., Szopa, S. and Zeng, G.: Preindustrial to present-day changes in tropospheric hydroxyl radical and methane lifetime from the Atmospheric Chemistry and Climate Model Intercomparison Project (ACCMIP), Atmos Chem Phys, 13(10), 5277–5298, doi:10.5194/acp-13-5277-2013, 2013.

Nemet, G. F., Holloway, T. and Meier, P.: Implications of incorporating air-quality co-benefits into climate change policymaking, Environ. Res. Lett., 5(1), 014007, doi:10.1088/1748-9326/5/1/014007, 2010.

Nenes, A. and Seinfeld, J. H.: Parameterization of cloud droplet formation in global climate models, J. Geophys. Res. Atmospheres 1984–2012, 108(D14), doi:10.1029/2002JD002911, 2003.

Olivié, D. J. L. and Peters, G. P.: Variation in emission metrics due to variation in CO2 and temperature impulse response functions, Earth Syst. Dyn., 4(2), 267–286, doi:10.5194/esd-4-267-2013, 2013.

Pierce, J. R., Chen, K. and Adams, P. J.: Contribution of primary carbonaceous aerosol to cloud condensation nuclei: processes and uncertainties evaluated with a global aerosol microphysics model, Atmospheric Chem. Phys., 7(20), 5447–5466, doi:10.5194/acp-7-5447-2007, 2007.

Pope, C. A., Burnett, R. T., Thun, M. J., Calle, E. E., Krewski, D., Ito, K. and Thurston, G. D.: Lung cancer, cardiopulmonary mortality, and long-term exposure to fine particulate air pollution, JAMA, 287(9), 1132–1141, 2002.

Pope, C. A., Burnett, R. T., Turner, M. C., Cohen, A., Krewski, D., Jerrett, M., Gapstur, S. M. and Thun, M. J.: Lung cancer and cardiovascular disease mortality associated with ambient air pollution and cigarette smoke: shape of the exposure-response relationships, Environ. Health Perspect., 119(11), 1616–1621, doi:10.1289/ehp.1103639, 2011.

Prather, M. J.: Numerical Advection by Conservation of 2nd-Order Moments, J. Geophys. Res.-Atmospheres, 91(D6), 6671–6681, 1986.

Rogelj, J., Meinshausen, M., Schaeffer, M., Knutti, R. and Riahi, K.: Impact of short-lived non-CO2 mitigation on carbon budgets for stabilizing global warming, Environ. Res. Lett., 10(7), 075001, doi:10.1088/1748-9326/10/7/075001, 2015.

Roman, H. A., Walker, K. D., Walsh, T. L., Conner, L., Richmond, H. M., Hubbell, B. J. and Kinney, P. L.: Expert Judgment Assessment of the Mortality Impact of Changes in Ambient Fine Particulate Matter in the U.S., Environ. Sci. Technol., 42(7), 2268–2274, doi:10.1021/es0713882, 2008.

Schmidt, G. A., Ruedy, R., Hansen, J. E., Aleinov, I., Bell, N., Bauer, M., Bauer, S., Cairns, B., Canuto, V., Cheng, Y., Del Genio, A., Faluvegi, G., Friend, A. D., Hall, T. M., Hu, Y., Kelley, M., Kiang, N. Y., Koch, D., Lacis, A. A., Lerner, J., Lo, K. K., Miller, R. L., Nazarenko, L., Oinas, V., Perlwitz, J., Perlwitz, J., Rind, D., Romanou, A., Russell, G. L., Sato, M., Shindell, D. T., Stone, P. H., Sun, S., Tausnev, N., Thresher, D. and Yao, M.-S.: Present-Day Atmospheric Simulations Using GISS ModelE: Comparison to In Situ, Satellite, and Reanalysis Data, J. Clim., 19(2), 153–192, doi:10.1175/JCLI3612.1, 2006.

Schmidt, G. A., Kelley, M., Nazarenko, L., Ruedy, R., Russell, G. L., Aleinov, I., Bauer, M., Bauer, S. E., Bhat, M. K., Bleck, R., Canuto, V., Chen, Y.-H., Cheng, Y., Clune, T. L., Del Genio, A., de Fainchtein, R., Faluvegi, G., Hansen, J. E., Healy, R. J., Kiang, N. Y., Koch, D., Lacis, A. A., LeGrande, A. N., Lerner, J., Lo, K. K., Matthews, E. E., Menon, S., Miller, R. L., Oinas, V., Oloso, A. O., Perlwitz, J. P., Puma, M. J., Putman, W. M., Rind, D., Romanou, A., Sato, M., Shindell, D. T., Sun, S., Syed, R. A., Tausnev, N., Tsigaridis, K., Unger, N., Voulgarakis, A., Yao, M.-S. and Zhang, J.: Configuration and assessment of the GISS ModelE2 contributions to the CMIP5 archive, J. Adv. Model. Earth Syst., 6(1), 141–184, doi:10.1002/2013ms000265, 2014.

Schnell, J. L., Prather, M. J., Josse, B., Naik, V., Horowitz, L. W., Cameron-Smith, P., Bergmann, D., Zeng, G., Plummer, D. A., Sudo, K., Nagashima, T., Shindell, D. T., Faluvegi, G. and Strode, S. A.: Use of North American and European air quality networks to evaluate global chemistry–climate modeling of surface ozone, Atmos Chem Phys, 15(18), 10581–10596, doi:10.5194/acp-15-10581-2015, 2015.

Seinfeld, J. H. and Pandis, S. N.: Atmospheric Chemistry and Physics, John Wiley and Sons, New York., 1998.

Shindell, D. and Faluvegi, G.: Climate response to regional radiative forcing during the twentieth century, Nat. Geosci., 2(4), 294–300, doi:10.1038/ngeo473, 2009.

Shindell, D., Faluvegi, G., Walsh, M., Anenberg, S. C., Van Dingenen, R., Muller, N. Z., Austin, J., Koch, D. and Milly, G.: Climate, health, agricultural and economic impacts of tighter vehicle-emission standards, Nat. Clim. Change, 1(1), 59–66, doi:10.1038/nclimate1066, 2011.

Shindell, D., Kuylenstierna, J. C. I., Vignati, E., van Dingenen, R., Amann, M., Klimont, Z., Anenberg, S. C., Muller, N., Janssens-Maenhout, G., Raes, F., Schwartz, J., Faluvegi, G., Pozzoli, L., Kupiainen, K., Hoeglund-Isaksson, L., Emberson, L., Streets, D., Ramanathan, V., Hicks, K., Oanh, N. T. K., Milly, G., Williams, M., Demkine, V. and Fowler, D.: Simultaneously Mitigating Near-Term Climate Change and Improving Human Health and Food Security, Science, 335(6065), 183–189, doi:10.1126/science.1210026, 2012.

Shindell, D. T., Faluvegi, G., Unger, N., Aguilar, E., Schmidt, G. A., Koch, D. M., Bauer, S. E. and Miller, R. L.: Simulations of preindustrial, present-day, and 2100 conditions in the NASA GISS composition and climate model G-PUCCINI, Atmospheric Chem. Phys., 6, 4427–4459, 2006.

Shindell, D. T., Pechony, O., Voulgarakis, A., Faluvegi, G., Nazarenko, L., Lamarque, J. F., Bowman, K., Milly, G., Kovari, B., Ruedy, R. and Schmidt, G. A.: Interactive ozone and methane chemistry in GISS-E2 historical and future climate simulations, Atmospheric Chem. Phys., 13(5), 2653–2689, doi:10.5194/acp-13-2653-2013, 2013a.

Shindell, D. T., Lamarque, J.-F. F., Schulz, M., Flanner, M., Jiao, C., Chin, M., Young, P. J., Lee, Y. H., Rotstayn, L., Mahowald, N., Milly, G., Faluvegi, G., Balkanski, Y., Collins, W. J., Conley, a. J., Dalsoren, S., Easter, R., Ghan, S., Horowitz, L., Liu, X., Myhre, G., Nagashima, T., Naik, V., Rumbold, S. T., Skeie, R., Sudo, K., Szopa, S., Takemura, T., Voulgarakis, a., Yoon, J.-H. H. and Lo, F.: Radiative forcing in the ACCMIP historical and future climate simulations, Atmospheric Chem. Phys., 13(6), 2939–2974, doi:10.5194/acp-13-2939-2013, 2013b.

Shindell, D. T., Lee, Y. and Faluvegi, G.: Climate and health impacts of US emissions reductions consistent with 2 °C, Nat. Clim. Change, advance online publication, doi:10.1038/nclimate2935, 2016.

Thompson, T. M., Rausch, S., Saari, R. K. and Selin, N. E.: A systems approach to evaluating the air quality co-benefits of US carbon policies, Nat. Clim. Change, 4(10), 917–923, doi:10.1038/nclimate2342, 2014.

Thomson, A. M., Calvin, K. V., Smith, S. J., Kyle, G. P., Volke, A., Patel, P., Delgado-Arias, S., Bond-Lamberty, B., Wise, M. A., Clarke, L. E. and Edmonds, J. A.: RCP4.5: a pathway for stabilization of radiative forcing by 2100, Clim. Change, 109(1-2), 77–94, doi:10.1007/s10584-011-0151-4, 2011.

United Nations Population Division: World Population Prospects: The 2010 Revision, CD-ROM Edition., 2011.

U.S. Environmental Protection Agency: Endangerment and cause or contribute findings for greenhouse gases under section 202(a) of the clean air act, [online] Available from:

http://www.epa.gov/climatechange/Downloads/endangerment/Endangerment_TSD.pdf (Accessed 6 November 2015), 2009.

U.S. Environmental Protection Agency: Air, Climate, and Energy, [online] Available from: http://www2.epa.gov/sites/production/files/2014-06/documents/strap-ace2012.pdf (Accessed 6 November 2015), 2012.

Vehkamaki, H., Kulmala, M., Napari, I., Lehtinen, K. E. J., Timmreck, C., Noppel, M. and Laaksonen, A.: An improved parameterization for sulfuric acid-water nucleation rates for tropospheric and stratospheric conditions, J. Geophys. Res.-Atmospheres, 107(D22), 4622, doi:DOI: 10.1029/2002JD002184, 2002.

Table 1. Summary of simulations used in this study.

Run type	Climate conditions	Emission year	Model	Length of run	Air quality and radiative forcing due to
FIXMET	2005	2005 2030 2055	ModelE2-OMA and ModelE2-TOMAS	3	Aerosols and non-CO_2 gases emissions
FUTURE	2030 RCP4.5 2055 RCP4.5	2030 2055	ModelE2-OMA	3	Aerosols, non-CO_2 gases, and GHGs emissions
INTERACT	2005	2005 2030 2055	ModelE2-OMA	20	Aerosols and non-CO_2 gas emissions and resulting atmospheric response (rapid adjustments)

Table 2. Concentration-Response Functions (CRF) used to compute mortality due to PM2.5 and ozone. LC stands for Lung cancer; CVD for Cardiovascular disease; RESP for respiratory disease and infections. See Section 3.2 for the details.

Species		LC	CVD/RESP	Notes
PM2.5	$CRF_{high,PM}$	RR = exp($\beta\Delta \ln C$) $\beta = a(=0.2322)*1.8$	RR = exp($\beta\Delta \ln C$) β =a(=0.1552)*1.8	a is from Chen et al. (2004).
	$CRF_{base,PM}$	RR = exp($\beta\Delta C$) β =log(1.14)/10*1.8	RR = exp($\beta\Delta C$) β =log(1.09)/10*1.8	The division by 10 is to apply numbers derived for 10 μg m^{-3} changes of PM2.5 to 1 μg m^{-3} changes.
	$CRF_{low,PM}$	RR=1+0.3195*(Inh*C)$^{0.7433}$ Inh= inhalation rate ($18m^{-3}$ d^{-1})	RR=1+0.2685*(Inh*C)$^{0.2730}$ Inh= inhalation rate ($18m^{-3}$ d^{-1})	1. Instead of ΔC, total concentration, C, is used. 2. RESP is not included.
Ozone	$CRF_{base,O3}$	N/A	RR = exp($\beta\Delta C$) β =log(1.04)/10	1. The division by 10 is to apply numbers derived for 10 ppb changes of ozone to 1 ppb changes. 2. Seasonal (6-month) maxima of daily 1-hr maxima ozone are used. 3. Only RESP is included.
	$CRF_{low,O3}$	N/A	RR = exp($\beta\Delta C$) β =1.11/10 for Cardiovasular disease β =0.47 for Respiratory Infections	1. ΔC is the change in daily O3. 2. The division by 10 is for increase in RR per a 10 ppb.

Table 3. Pair of the FIXMET simulations used to compute the impact of policies. In the "Simulations" column, the first letters represent the US emission scenarios and the last two numbers represent the emission year ("bs" for the baseline, "noaq" for the no air quality regulations, "c50" for the 50% CO_2 cap in the baseline, and "c50nq" for the 50% CO_2 cap in the noaq scenario).

Impact of	Simulations	Short name
Air quality regulation	(bs30– bs05) – (noaq30 – noaq05)	AQ30
	(bs55– bs05) – (noaq55 – noaq05)	AQ55
CO_2 reduction policy	(c5030-c5005) –(bs30-bs05)	$CO_2$30
	(c5055-c5005) –(bs55-bs05)	$CO_2$55
CO_2 reduction policy w/o	(c50nq30- c50nq05) – (noaq30 –noaq05)	CO_2NQ30
air quality regulation	(c50nq55- c50nq05) – (noaq55 –noaq05)	CO_2NQ55
Air quality regulation and	(c5030-c5005) – (noaq30-noaq05)	BOTH30
CO_2 reduction policy	(c5055-c5005) – (noaq55-noaq05)	BOTH55

Table 4. Changes in the US mean air pollution in 2030 and 2055 in respect to 2005 (averaged over the 50 states) due to the air quality regulations and CO_2 reduction policy that are divided by the model baseline 2005 (bs05) level.

Species	bs05 level [μg m^{-3} or ppb]	(2030 – 2005)/bs05 [%]				(2055-2005)/bs05 [%]			
		$CO_2$30	CO_2NQ30	AQ30	BOTH30	$CO_2$55	CO_2NQ55	AQ55	BOTH55
PM2.5	8.5	-1.5	-4.2	-20.4	-21.9	-4.1	-9.6	-22.6	-26.6
SO_4	1.2	-9.2	-28.9	-44.4	-53.6	-12.3	-45.2	-46.8	-59.1
EC	0.25	6.4	6.6	-50.2	-43.8	2.2	3.3	-59.0	-56.8
OM	1.3	1.2	1.0	-27.0	-25.9	-3.7	-7.7	-31.9	-35.6
NO_3	1.4	-3.6	-3.9	-54.5	-58.1	-11.6	-14.8	-59.8	-71.4
NO_X	3.2	2.6	1.1	-61.2	-58.6	-1.6	-13.0	-68.9	-70.5
O_3	57	1.2	1.0	-14.6	-13.4	0.1	-2.0	-15.2	-15.1
CO	174	0.1	0.0	-10.7	-10.6	-2.0	-7.2	-12.5	-14.5

Figure 1. Emission plots of the four GLIMPSE US scenarios. See Section 2 for the details.

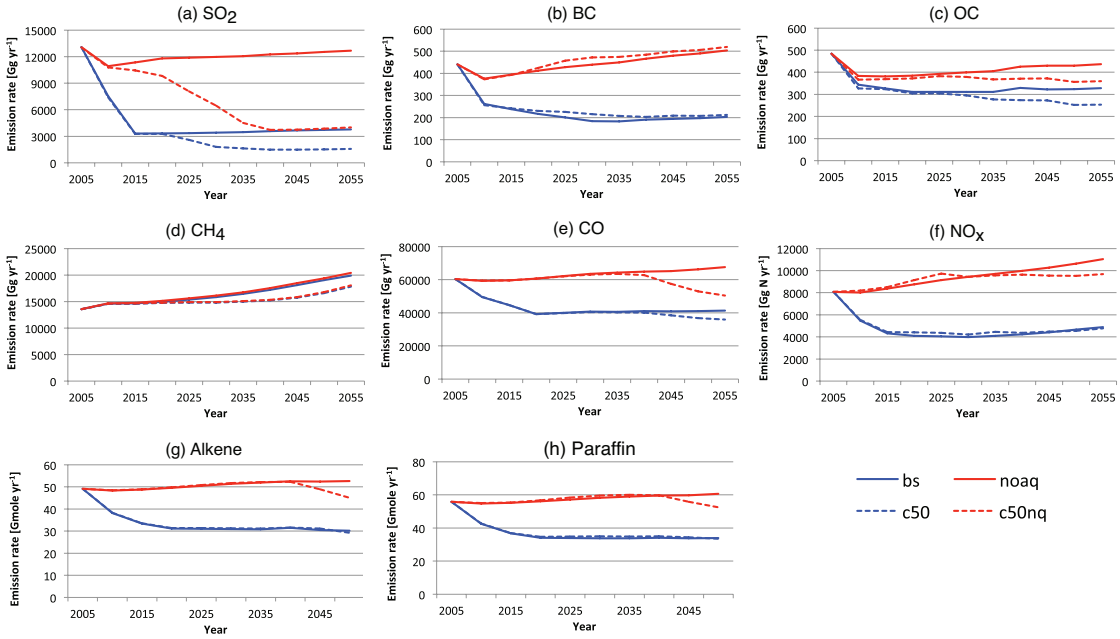

Figure 2. Changes in the US mean air pollution in 2030 and 2055 respect to 2005 due to the air quality regulations and CO_2 reduction policy (averaged over the 50 U.S states). All PM has a unit of $\mu g\ m^{-3}$, and gases have a unit of ppb. O_3 and CO are multiplied by 0.1 to plot in the same Y-axis scale as others. See S-Table 2 in the supplementary materials for the exact values.

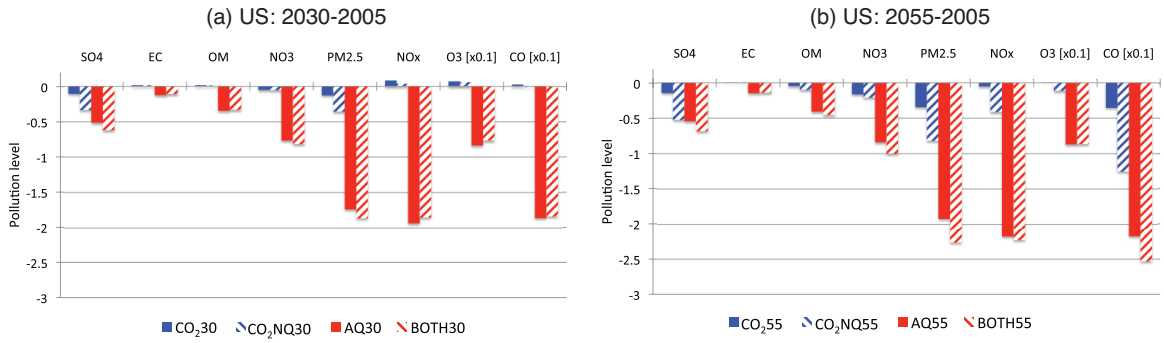

Figure 3. Spatial distributions of changes in surface PM and gas pollutants concentrations due to impact of (a-h) the air quality regulations (AQ30) and (i-p) CO_2 reduction policy ($CO_2$30).

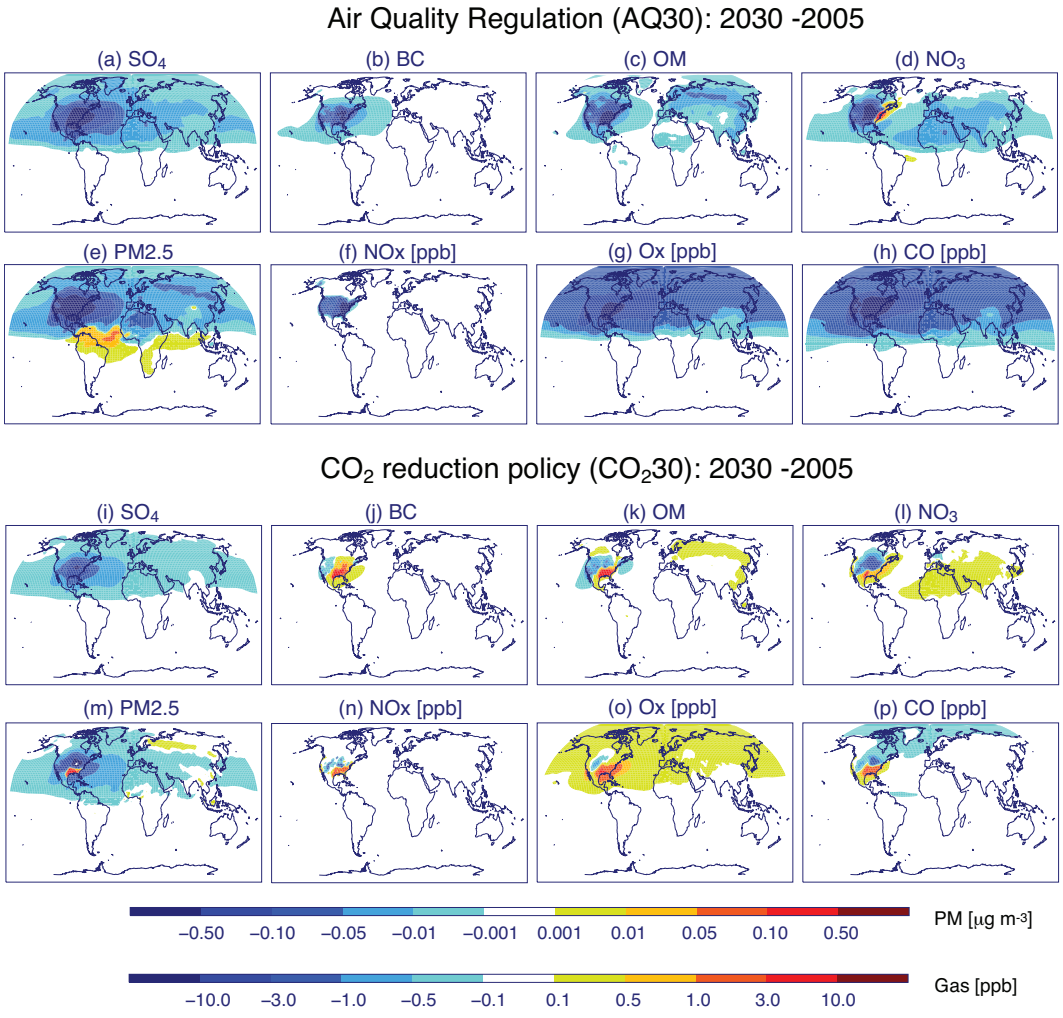

Figure 4. Same as Figure 2 but for the difference between ModelE2-TOMAS and ModelE2-OMA. See S-Table 3 in the supplementary materials for the exact values for ModelE2-TOMAS.

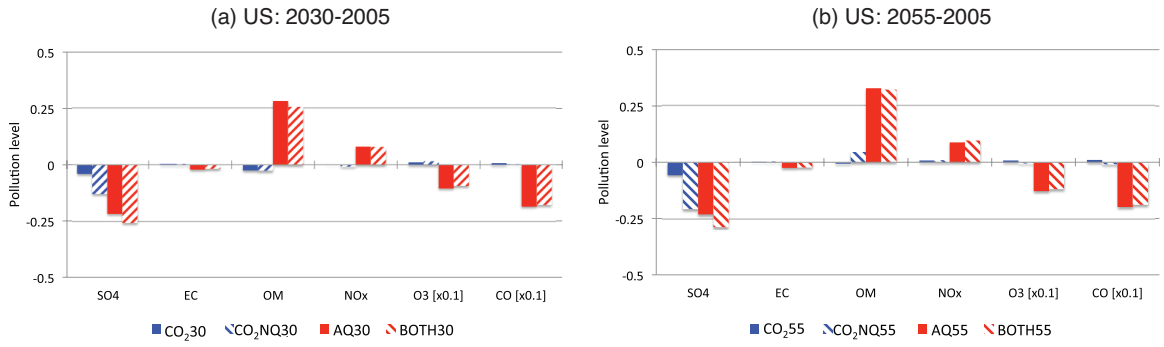

Figure 5. Impact of the air quality regulations and CO_2 reduction policy on U.S. mortality related to PM2.5. Colorbar shows the mortality rate using $CRF_{base,PM}$. The higher ($CRF_{high,PM}$) and lower ($CRF_{low,PM}$) bars indicate the spread in mortality change predicted using the range of concentrations-response functions used in the study (see Table 2). Note that the x-axis is log-scale and has a unit of thousand people per year. The total mortality rate using $CRF_{base,PM}$ is presented in the right side.

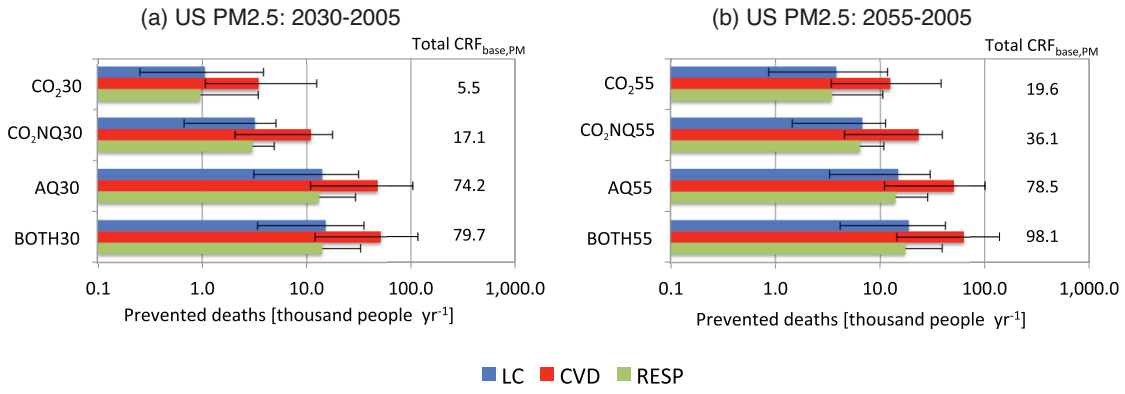

Figure 6. Impact of the air quality regulations and CO_2 reduction policy on U.S. mortality related to ozone. Important note that colorbar shows the mortality rate using $CRF_{low,O3}$, and the horizontal upper bars are for mortality rates using $CRF_{base,O3}$ because $CRF_{base,O3}$ only include RESP. It has a unit of thousand people per year. The total mortality rate using $CRF_{base,O3}$ is presented in the right side.

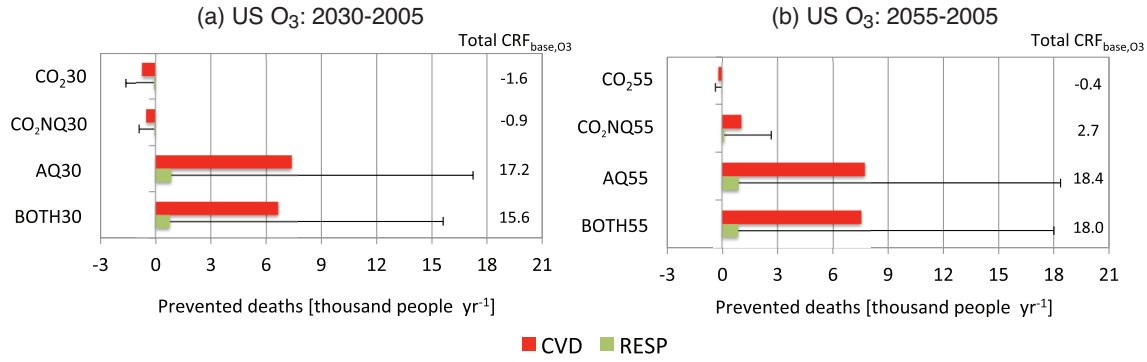

Figure 7. Global distributions of prevented PM- and O_3-related mortality due to impact of (a and b) the air quality regulations in 2030 (AQ30), (d and e) CO_2 reduction policy in 2030 ($CO_2$30), and (g and h) CO_2 reduction policy in 2055 ($CO_2$55). The differences between two aerosol models are shown in (c) for AQ30, (f) for $CO_2$30, and (i) for $CO_2$55. In each panel, globally summed mortality is presented in the right upper corner.

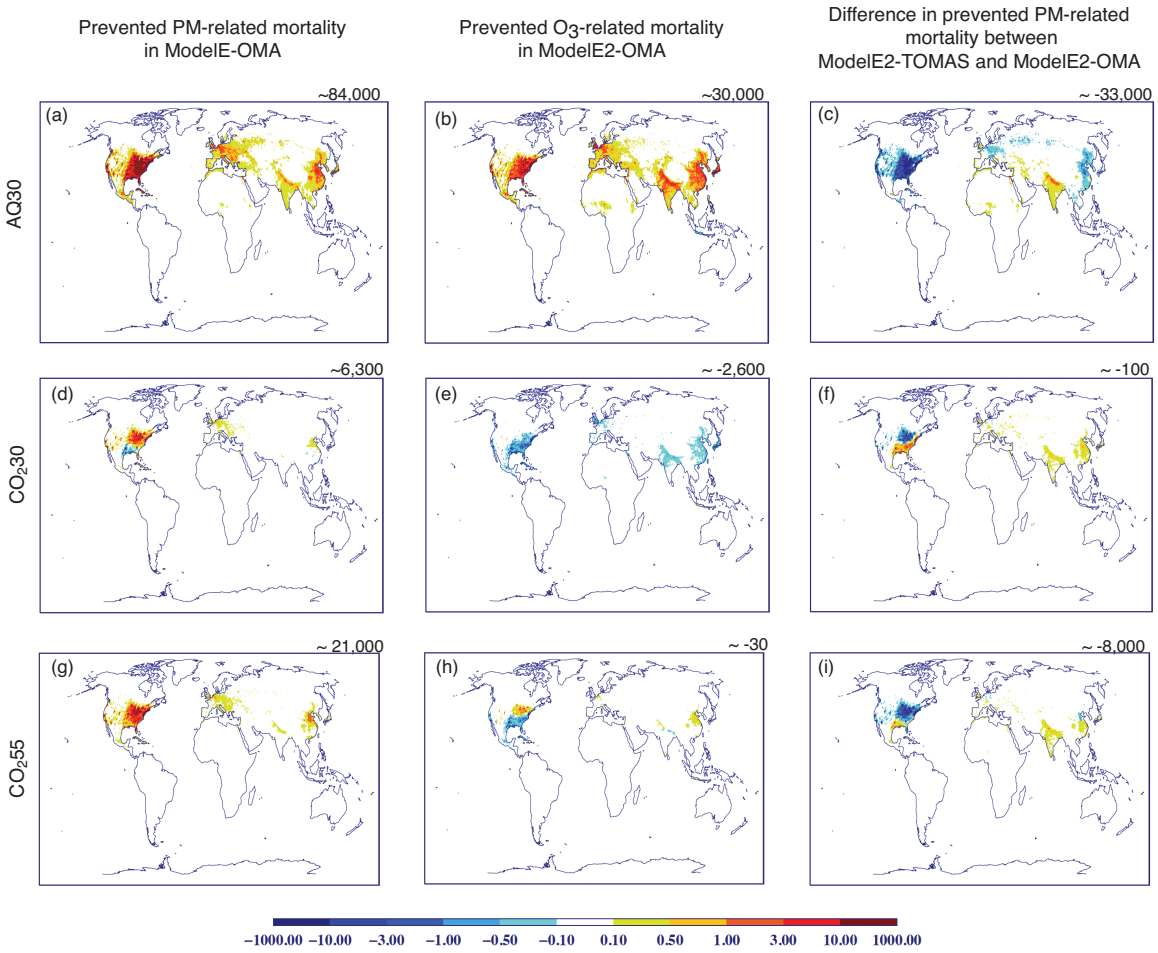

Figure 8. Same as Figure 5 but for the difference between ModelE2-TOMAS and ModelE2-OMA.

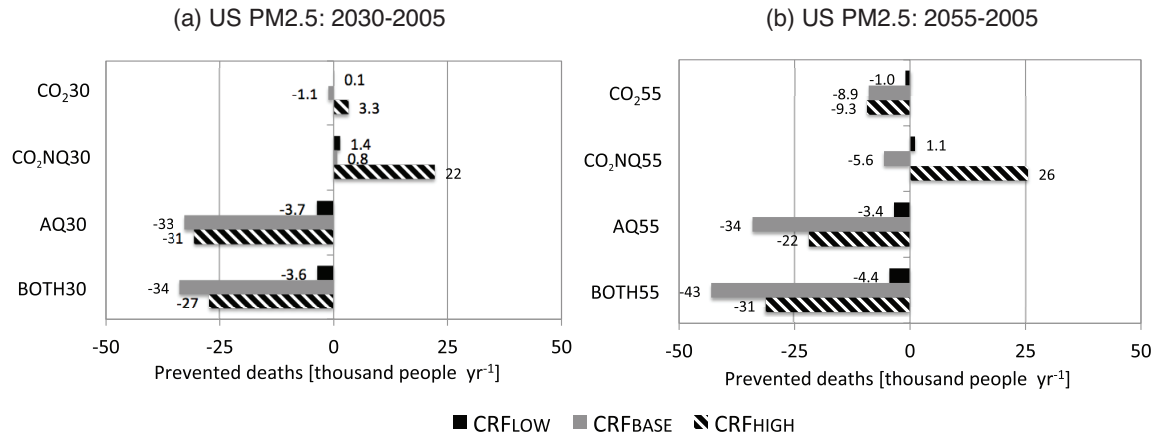

Figure 9. Impact of the air quality regulations and CO_2 reduction policy on global (a and b) and U.S. (c and d) averaged radiative forcings in 2030 and 2055 relative to 2005. Note that BC-albedo forcing is added into aerosol direct forcing (ADF). The exact value of RFs is presented in S-Tables 5 and 6 for global mean and US mean, respectively.

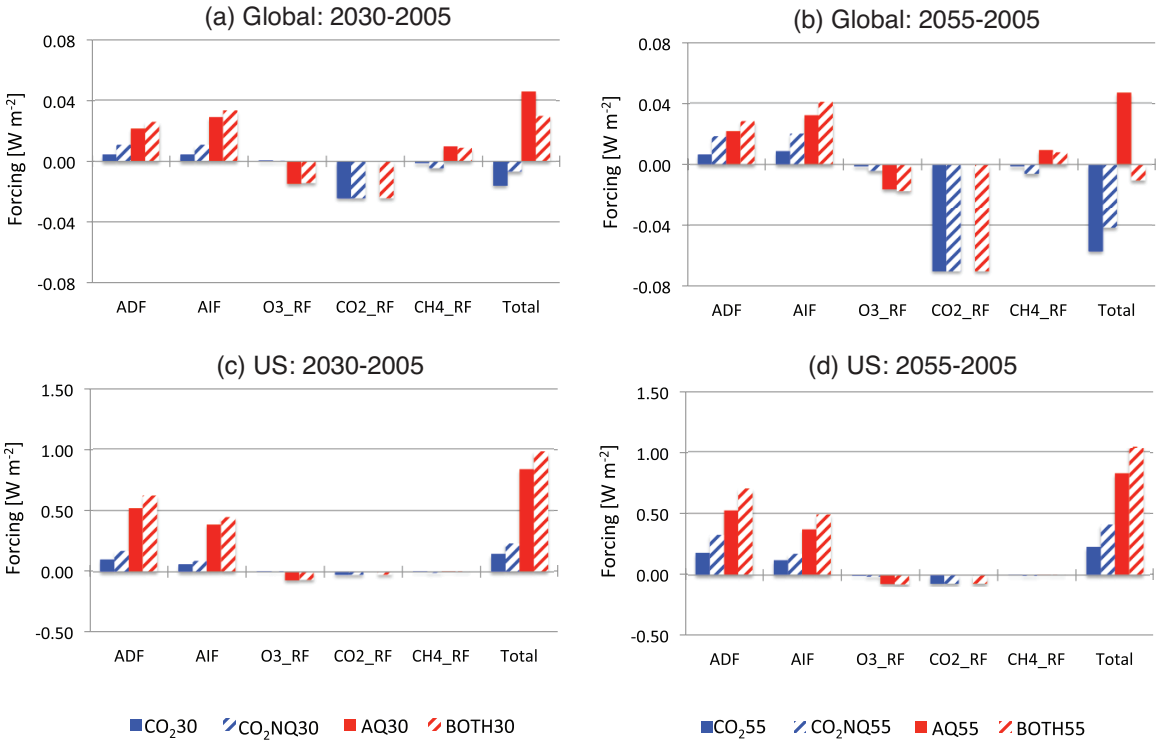

Figure 10. Impact of the CO_2 reduction policy ($CO_2$30) on radiative forcing in 2030 relative to 2005.

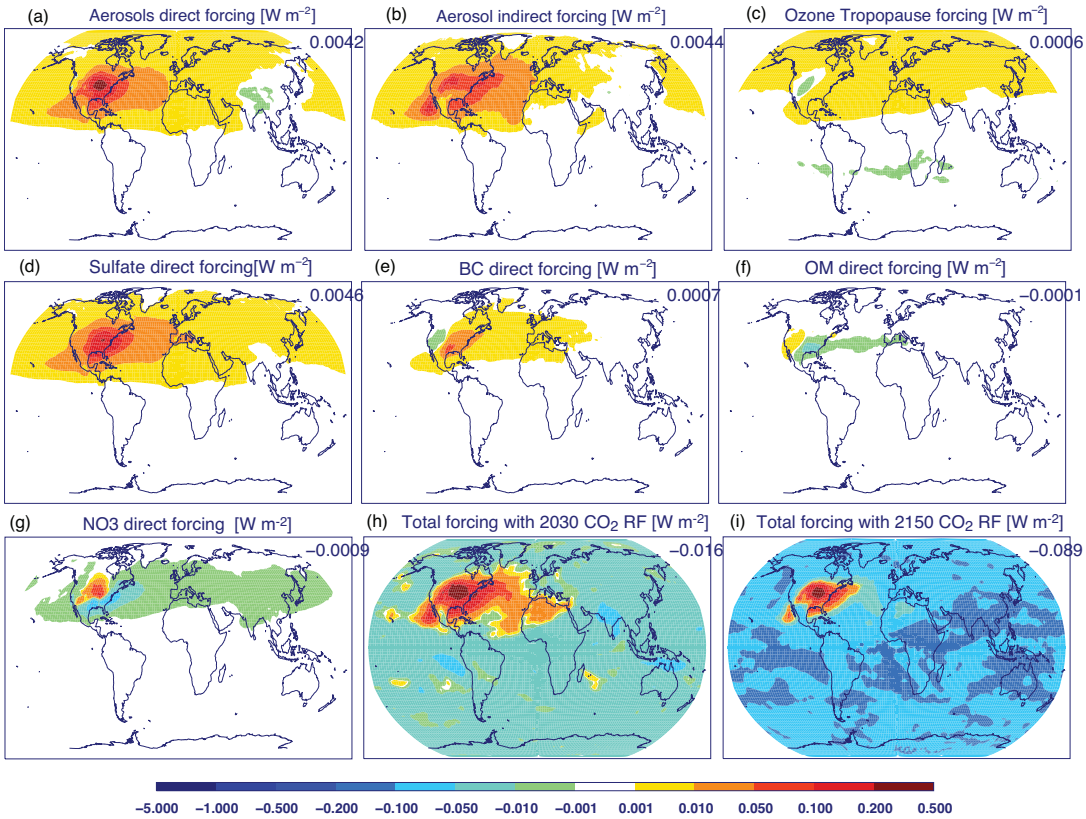

Figure 11. Impact of the air quality regulations (AQ30) on radiative forcing in 2030 relative to 2005.

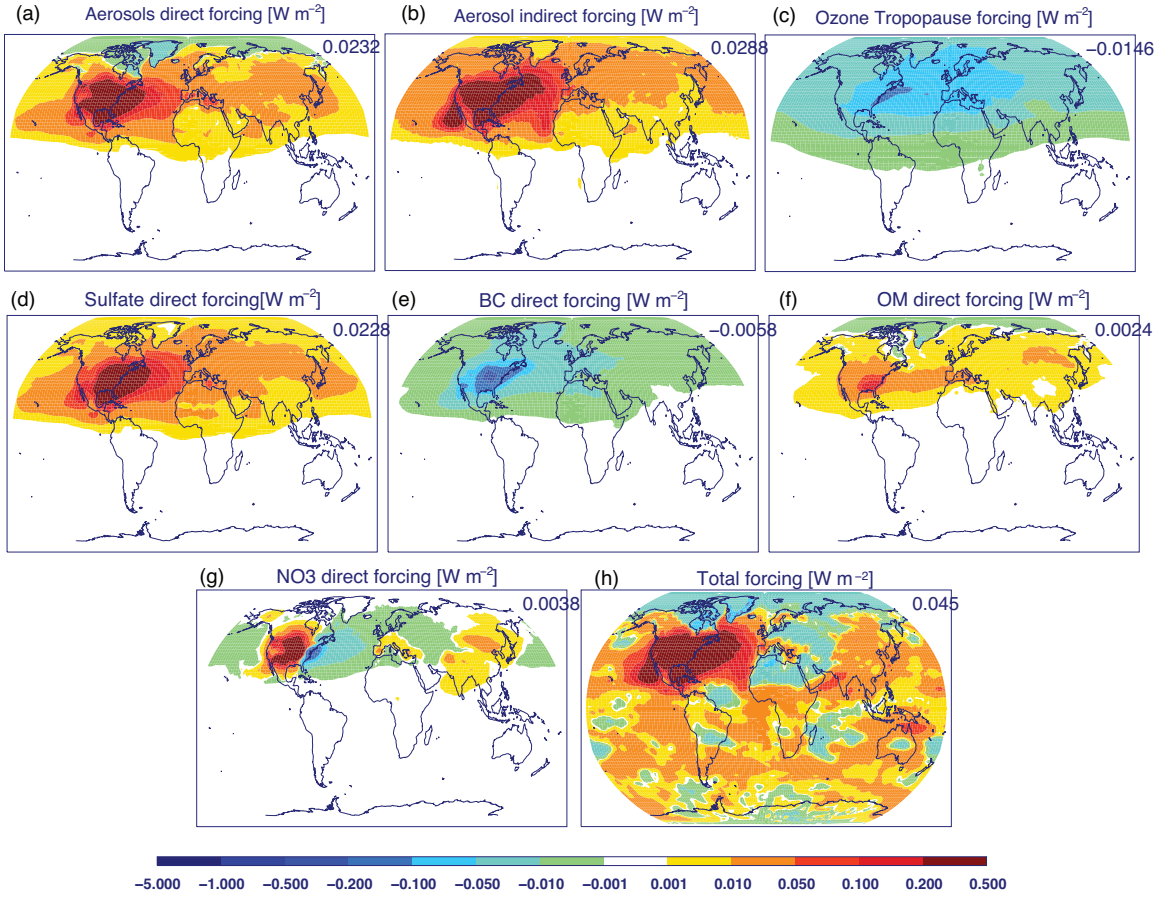

Figure 12. Same as Figure 9 but for the difference in the US mean between ModelE2-TOMAS and ModelE2-OMA.

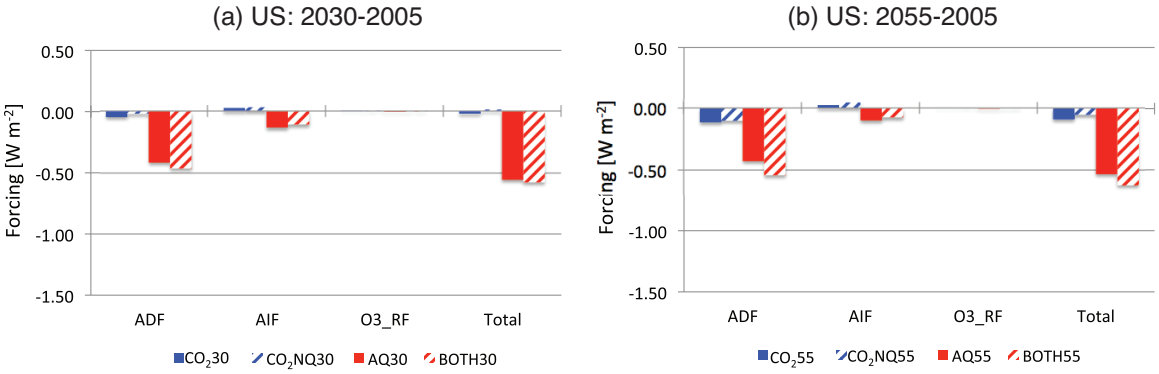

Figure 13. Impact of future warm climate conditions on U.S. averaged radiative forcings in (a) 2030 and (b) 2055 relative to 2005. Note that BC-albedo forcing is added into aerosol direct forcing (ADF).

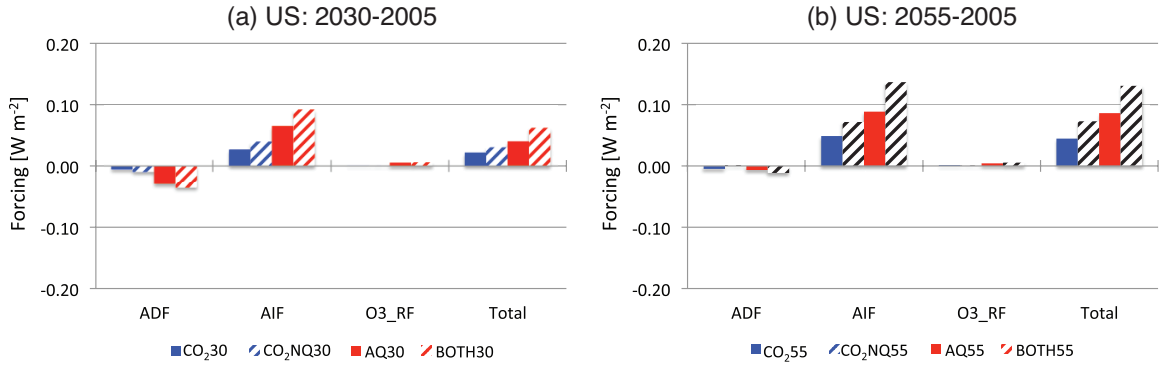

Figure 14. Impact of climate response due to emissions on U.S. averaged radiative forcings in (a) 2030 and (b) 2055 relative to 2005. Note that BC-albedo forcing is added into aerosol direct forcing (ADF).